NONLINEAR MODELLING OF CHEMICAL KINETICS FOR THE ACID MINE DRAINAGE PROBLEM AND RELATED PHYSICAL TOPICS

MEND Project 1.51.2

This work was done on behalf of MEND and sponsored by Environment Canada

October 1993

NONLINEAR MODELLING OF CHEMICAL KINETICS FOR THE ACID MINE DRAINAGE PROBLEM AND RELATED PHYSICAL TOPICS

FINAL REPORT
Submitted to the
British Columbia Acid Mine
Drainage Task Force

by

J.A. Tuszyński*, M.L.A. Nip and D. Sept*

Department of Physics
University of Alberta
Edmonton, Alberta, T6G 2J1

* present address:
Institut für Theoretische Physik I
Heinrich-Heine Universität Düsseldorf
D-40225 Düsseldorf

Contents

Summary

The problem of Acid Mine Drainage (AMD) poses a significant environmental danger in British Columbia and other parts of the world involved in mining activities. Oxygenation reactions responsible for the chemical generation of acidity have been, by and large, identified. Thus far rather simplified modelling techniques have been used in the analysis of these complex reactions that possess feedback loops characteristic of chemical chaos systems. Our primary objective was to provide an in-depth study of the basic reactions in the AMD problem; to model the associated chemical kinetics and draw conclusions regarding the predictability of these nonlinear processes.

Having derived the constituent differential equations under several sets of conditions we have applied modern analytical and numerical techniques to investigate the regimes of behavior for both acid production and neutralization reactions. We have discussed important factors in the determination of predictable and unpredictable ranges of behavior which should be of much use in the prevention program. In the final two sections of the report an outlook has been given for the next logical steps in the modelling of chemical kinetics for the AMD problem. The report is supplemented with six Appendices that give the reader an overview of nonlinear phenomena.

Sommaire

Le problème du drainage minier acide (DMA) pose un risque sérieux de dommage environnemental en Colombie-Britannique et dans d'autres endroits au monde où se pratiquent des activités liées à l'exploitation minière. Généralement parlant, on a déterminé les réactions d'oxygénation qui résultent dans la production chimique d'acidité. Jusqu'à ce jour, des techniques de modélisation plutôt simples ont été utilisées pour analyser ces réactions complexes qui ont des boucles de rétroaction qui caractérisent les systèmes de chaos chimique. Notre premier objectif était d'effectuer une étude exhaustive des réactions de base inhérentes au problème du DMA; d'élaborer un modèle de la cinétique de réaction chimique qui lui est associée et de tirer des conclusions au sujet de la prévisibilité de ces processus non linéaires.

Après avoir élaboré dans diverses conditions les équations différentielles appropriées, nous avons utilisé des techniques numériques et analytiques modernes pour étudier les modes de comportement dans le cas de la production d'acide et celui des réactions de neutralisation. Nous avons examiné les éléments importants afin de déterminer les modes de comportement prévisibles et imprévisibles, susceptibles d'être utilisés aux fins du programme de prévention. Dans les deux derniers articles du rapport, nous donnons un aperçu des nouvelles étapes logiques de la modélisation de la cinétique de réaction chimique du DMA. Le rapport comprend également six annexes qui donnent au lecteur un aperçu des phénomènes non linéaires.

Section 1

Introduction

One of the major sources of environmental concern related to mining in general, and to coal mining in particular, has been the so-called acid rock drainage (ARD). This term describes contamination resulting from waste rock materials which contain such sulphide minerals as, for example, pyrite and pyrrhotite. Natural oxygenation of sulphide minerals occurs in rock which is exposed to air and water. Acidic drainage, if not neutralized by such constituents as limestone and dolomite, may in general be generated [ARDPM] from the following sources: (a) underground workings, (b) open pit mine walls, (c) waste rock dumps, (d) ore stockpiles and (e) tailings impoundments. Once ARD formation has been initiated, the process is very difficulty to arrest. Of course, the presence of alkaline rocks may lead to a reduction in ARD by providing a neutralization potential. It should be mentioned that ARD is a world-wide problem in mining operations and its impact on the environment can be quite severe due to the toxicity of heavy metals and other products as has been witnessed, for example, in Norway.

It is, therefore, extremely important to understand the processes involved in the ARD formation so that protective measures can be taken early in time. The most cost-effective method of reducing the impact of ARD is accurate prediction. However, as will be discussed later in this report, the complexity of the chemical reactions involved precludes an easy and simple approach to the problem of prediction. The chemical processes are not only strongly dependent on external conditions (such as the prevailing weather conditions) and the geology of the terrain but, perhaps more importantly, they involve feedback loops making the problem inherently nonlinear. Competition between neutralization and acid potential complicates the problem even more. To the best of our knowledge, most of the earlier models studied in this connection did not include this aspect in their analyses. A notable exception of modeling that included competition between acid generation and neutralization are the studies of Scharer et al. (1993) exploring models for tailings and Jaynes et al. (1984) in regard to coal spoils. We believe that any accurate model must account for this aspect to be successful.

This project has been chiefly concerned with the modelling of nonlinear kinetics of the chemical reactions present in both acid production and neutralization that are associated with the ARD processes. Since the conceptual framework involved is based on a range of novel scientific ideas, we have decided to include a section that deals exclusively with a pedestrian-level explanation of these important concepts. We discuss later in the text and in the Appendices nonlinear kinetic equations, phase-space descriptions, limit cycles, chaos and fractality, all of which are of significance to the problem studied. They will

play a key role in the modelling techniques employed later on to the chemistry of the ARD processes. The following section provides an overview of the ARD chemistry to the extent available in the literature on this topic. The main part of the report then follows and it addresses the questions of:

(a) Deriving the equations of chemical kinetics for both acid production and acid neutralization reactions. (The presence of reverse reactions and inflow-outflow conditions will be discussed separately in this context.)

(b) Solving the derived equations under a range of conditions that are model dependent.

(c) Setting up and solving kinetic equations that effectively include the porous nature of the rock medium.

The final section of the report is a discussion of the obtained results and of the need for further improvements in the modelling techniques. Of particular importance will be the requirement to account for the inhomogeneity of the medium. This will lead us to propose a modern approach that includes the fractal character of the porous rock structure.

Section 2

Nonlinear Chemical Kinetics

2.1 Homogeneous Media

In this subsection we develop our primary topic of interest, i.e. the modelling of nonlinear chemical reactions. The reader is referred to the Appendices for general information on the role of nonlinearity which may be necessary in order to properly analyze the complexity of the problem at hand. The important factor in our discussion will be the presence of autocatalytic reactions. As one of the simplest examples imaginable consider the reaction:

$$A + 2B \xrightarrow{k} 3B \tag{2.1}$$

where k is the reaction rate and it is assumed that the reaction takes place in a continuous-flow stirred reactor as shown below.

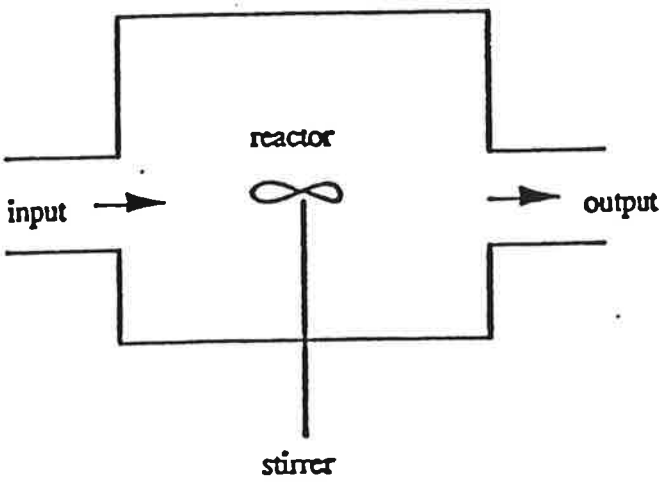

Figure 2.1: A schematic of a continuous-flow stirred reactor.

Denoting the concentrations of the chemical species A and B as a and b, respectively, we find the relevant equations describing the time evolution of $a(t)$ and $b(t)$ as

$$\frac{da}{dt} = -kab^2 \tag{2.2}$$

$$\frac{db}{dt} = kab^2 \tag{2.3}$$

If we allow reverse reactions to take place at a rate k^-, so that the equilibrium constant for the formation of A from B is $E = k^-/k$, i.e. we have [Gray (1988)]

$$A + 2B \underset{k^-}{\overset{k}{\rightleftharpoons}} 3B \tag{2.4}$$

the corresponding equations now take the form

$$\frac{da}{dt} = -kab^2 + k^-b^3 \tag{2.5}$$

$$\frac{db}{dt} = kab^2 - k^-b^3 \tag{2.6}$$

We note here that the terms on the right-hand sides above are proportional to the product of the concentrations corresponding to each type of the molecular species reacting.

An additional feature of these types of reactions may be the presence of flows through the tank. If the net outflow rate is k_f where:

$$k_f = \text{outflow rate/reactor volume}$$

then the time evolution equations take the final form

$$\frac{da}{dt} = k_f(a_o - a) - kab^2 + k^-b^3 \tag{2.7}$$

$$\frac{db}{dt} = k_f(b_o - b) + kab^2 - k^-b^3 \tag{2.8}$$

where a_o and b_o represent reactant concentrations at the input port of the two species involved.

A very well studied example of a potentially chaotic chemical reaction is the Belousov-Zhabotinskii reaction [Baker et al. (1990)]

$$A + B \underset{k_r}{\overset{k_f}{\rightleftharpoons}} C \tag{2.9}$$

carried out in a container with a flow rate r for reactants A and B. The governing equations are

$$\frac{dA}{dt} = -k_fAB + k_rC - r(A - A_o) \tag{2.10}$$

$$\frac{dB}{dt} = -k_fAB + k_rC - r(B - B_o) \tag{2.11}$$

$$\frac{dC}{dt} = +k_fAB - k_rC - rC \tag{2.12}$$

where A_o and B_o are the respective reactant concentrations at the input port. If $r = 0$, the reaction proceeds to equilibrium. If r is large, the materials are exhausted from the

container before they have time to react. However, for *intermediate* values of r the system exhibits both chaotic and time-periodic states. The important aspect to point out is the open nature of the reactor and the rate of flow r as a control parameter. Experimental studies confirming these predictions abound and they involve catalytic reactions, enzyme reactions and another important example, the decomposition of SO_4^{2-}. They were observed both in homogeneous and surface catalytic reactions [Cvitanović (1984)]. The important factors are the autocatalytic character of the reactions through a feedback mechanism [Glansdorff et al. (1971)] and the stirring process that maintains homogeneity.

Let us consider two more examples which are intended to illustrate different types of behavior. The three coupled reactions below [Glansdorff et al. (1971)] described by the reaction chain

$$A + X \underset{k_{-1}}{\overset{k_1}{\rightleftharpoons}} 2X \tag{2.13}$$

$$X + Y \underset{k_{-2}}{\overset{k_2}{\rightleftharpoons}} 2Y \tag{2.14}$$

and

$$Y \underset{k_{-3}}{\overset{k_3}{\rightleftharpoons}} E \tag{2.15}$$

include two autocatalytic steps (the first and second reactions) and an uncatalyzed conversion (the third step). The global reaction is $A \rightleftharpoons E$ and the equilibrium concentrations are:

$$\left(\frac{A}{E}\right)_{eq} = \frac{k_{-1}k_{-2}k_{-3}}{k_1k_2k_3}; \quad X_{eq} = \frac{k_1}{k_{-1}}; \quad Y_{eq} = \frac{k_1k_2}{k_{-1}k_{-2}}A. \tag{2.16}$$

Neglecting the inverse reactions ($k_1 = k_2 = k_3 = 0$) gives the kinetic equations in the form

$$\frac{dX}{dt} = k_1AX - k_2XY \tag{2.17}$$

$$\frac{dY}{dt} = k_2XY - k_3Y. \tag{2.18}$$

Their analysis yields a single non-vanishing steady-state with

$$X_o = \frac{k_3}{k_2}; \qquad Y_o = \frac{k_1}{k_2}A \tag{2.19}$$

which supports stable periodic oscillations around this focus point. They are represented by

$$X(t) = X_o + xe^{i\omega t}; \qquad Y(t) = Y_o + ye^{i\omega t} \tag{2.20}$$

with the oscillation frequency: $\omega = \pm\sqrt{k_1k_3A}$.

However, a different picture emerges when we investigate the following system of four reactions:

$$A \underset{k_{-1}}{\overset{k_1}{\rightleftharpoons}} X \tag{2.21}$$

$$2X + Y \underset{k_{-2}}{\overset{k_2}{\rightleftharpoons}} 3X \tag{2.22}$$

$$B + X \underset{k_{-3}}{\overset{k_3}{\rightleftharpoons}} Y + D \tag{2.23}$$

and

$$X \underset{k_{-4}}{\overset{k_4}{\rightleftharpoons}} E \tag{2.24}$$

where the second step is autocatalytic. The overall reaction is: $A + B \rightleftharpoons E + D$ and the equilibrium conditions give

$$X_{eq} = \frac{k_1 A}{k_{-1}};\ Y_{eq} = \frac{k_{-2}k_1}{k_2 k_{-1}}A;\ \frac{E}{A} = \frac{k_1 k_4}{k_{-1}k_{-4}};\ \frac{D}{B} = \frac{k_2 k_3}{k_{-2}k_{-3}}. \tag{2.25}$$

Assuming for simplicity that $k_1 = k_2 = k_3 = k_4 = 1$ and $k_{-1} = k_{-2} = k_{-3} = k_{-4} = k$, we obtain the kinetic equations as

$$\frac{dX}{dt} = A + X^2Y - BX - X + k(YD + E - X - X^3) \tag{2.26}$$

and

$$\frac{dY}{dt} = BX - X^2Y + k(X^3 - YD). \tag{2.27}$$

The steady-state solution is

$$X_o = \frac{A + kE}{1 + k}; \qquad Y_o = \frac{kX_o^2 + B}{X_o^2 + kD}X_o. \tag{2.28}$$

Normal mode analysis for these coupled equations leads to a new behavior characterized by an instability of periodic oscillations about the steady state beyond the critical value of B which is $B_c = 1 + A^2$. For $B < B_c$ a limit cycle replaces a focus point as a stable solution in a process called a bifurcation.

The behavioral patterns discovered by Prigogine and his associates are characteristic of a class of multidimensional vectorial evolution equations of the type

$$\frac{d\mathbf{x}}{dt} = f(\mathbf{x}) \tag{2.29}$$

where $f(\mathbf{x})$ is a nonlinear function of $\mathbf{x}$ and $\mathbf{x} = (\mathbf{x_1}, \mathbf{x_2}, \ldots, \mathbf{x_n})$ represents the concentrations involved. The objective in their study is to find stable attractors and determine possible bifurcations [Glass et al. (1988)]. The use of Lyapunov theory of stability is of great help.

These models have been extended to a much larger chain of coupled reactions, for example 7 in ref. 12. State-of-the-act computer codes can handle up to 20 coupled variables but, in most cases, the main features can be obtained by studying several (typically three) skeleton reactions (e.g. the Oregonator). The observed behavior usually indicates the existence of periodic regimes with their basins of attraction as well as regions of chaotic behavior and intermittency. Therefore, depending on the details of initial conditions and control parameters the system *may or may not* be predictable [Vidal et al. (1984)].

2.2 Reactions in Porous Media

Very recently, applications of Prigogine's theory have been extended to heterogeneous reactions in porous materials which is of particular importance to geochemistry [Kopelman (1986)]. The key to the modelling of such reactions is to evaluate the size of the effectively explored space per unit time, i.e. the efficiency of the random walker (reactant). The actual exploration volume of the random walker, denoted S, is a fractal object whose effective volume grows only (approximately) as $V^{2/3}$ where V is the diffusion space volume. Here, $V = \frac{4}{3}\pi r^3$ where $r = Dt$ and D is the diffusion constant. If the molecules execute coherent motion or if the exploration space is isotropic, then $S \sim t$ and, as a result, the reaction rate k is constant since $k \sim dS/dt$. The latter quantity, dS/dt, is also referred to as the efficiency of the walker. However, for locally heterogeneous media (e.g. porous media), the exploration volume S is a function of time characterizing the medium. It was found through computer experiments that in general

$$S \sim t^{d_s/2} \tag{2.30}$$

where d_s is the spectral dimension of the fractal medium. Consequently, the reaction rate is

$$k \sim t^{-h} \tag{2.31}$$

where $h = 1 - \frac{d_s}{2}$ if $d_s < 2$, and $h = 0$ if $d_s > 2$. In particular, for a homogeneous medium, $d = d_s = 3$ and $h = 0$ giving a constant reaction rate, as expected. It was also found [Kopelman (1986)] that in the case of a one-dimensional pore ($d = d_s = 1$), $h = \frac{1}{2}$. More importantly, perhaps, for percolating clusters in both $d = 2$ and $d = 3$, $d_s = \frac{4}{3}$ and consequently $h = \frac{1}{3}$. The same is true for diffusion-limited aggregation and for a random fractal. In our applications to the AMD problem we will therefore use the latter result and assume in our simulations that $k \sim t^{-1/3}$ in order to account for the porosity of the medium.

Section 3

The Chemical Processes in AMD

3.1 Introductory Comments

Acid generation is caused by the exposure of rock containing sulphide minerals, principally pyrite (FeS_2) to oxygen and water. This results in the production of acidity and elevated concentrations of sulphate and metals as a consequence of the oxidation of sulphur in the mineral to a higher oxidation state and the precipitation of ferric ion water hydroxide, if possible.

The ability of a particular rock sample to generate acidity is dependent on the relative content of acid generating minerals and acid consuming ones. The latter ones participate in the process of neutralization. Both acid generation and acid neutralization are complex multi-step chemical reactions with complicated behavior that depends on many external and internal factors. The net effect in the process of ARD is determined by the balance between (a) acid generation caused by the exposure of sulphide minerals in rock to air and water and (b) neutralization of acid upon contact with acid-consuming minerals.

The oxygenation reactions are often accelerated by biological activity which is very significant (see Fig. 3.1) but at this stage we will not attempt to include this aspect in our analysis. Crystalline substances which contain sulphur combined with a metal or a semi-metal but no oxygen are called sulphide minerals and below we list some of the most commonly found [Glansdorff et al. (1971)]: pyrite (FeS_2) and pyrrhotite ($Fe_{1-x}S$) which play the most dominant role, as well as several less important sulphides such as marcarite (FeS_2), smythite, greigite (Fe_3S_4), mackinawite (FeS), chalcocite (Cu_2S), etc. In the analysis below we practically assume that only pyrite is responsible for AMD processes. The reactions triggered yield low pH water which can mobilize heavy metals contained in the waste rock and its surroundings. Through water transport the resultant drainage carries elevated metal levels and sulphate into the receiving environment.

3.2 Acid Generation

The main pathway to acid generation involves pyrite (FeS_2) and its chemistry is known to occur through the following stages: [DARDTG v.1]

(1) direct oxidation of the sulphide mineral into dissolved iron, sulphate and hydrogen

$$FeS_2(s) + \frac{7}{2}O_2(g) + H_2O \xrightarrow{k_1} Fe^{2+} + 2SO_4^{2-}(aq) + 2H^+(aq) \qquad (3.1)$$

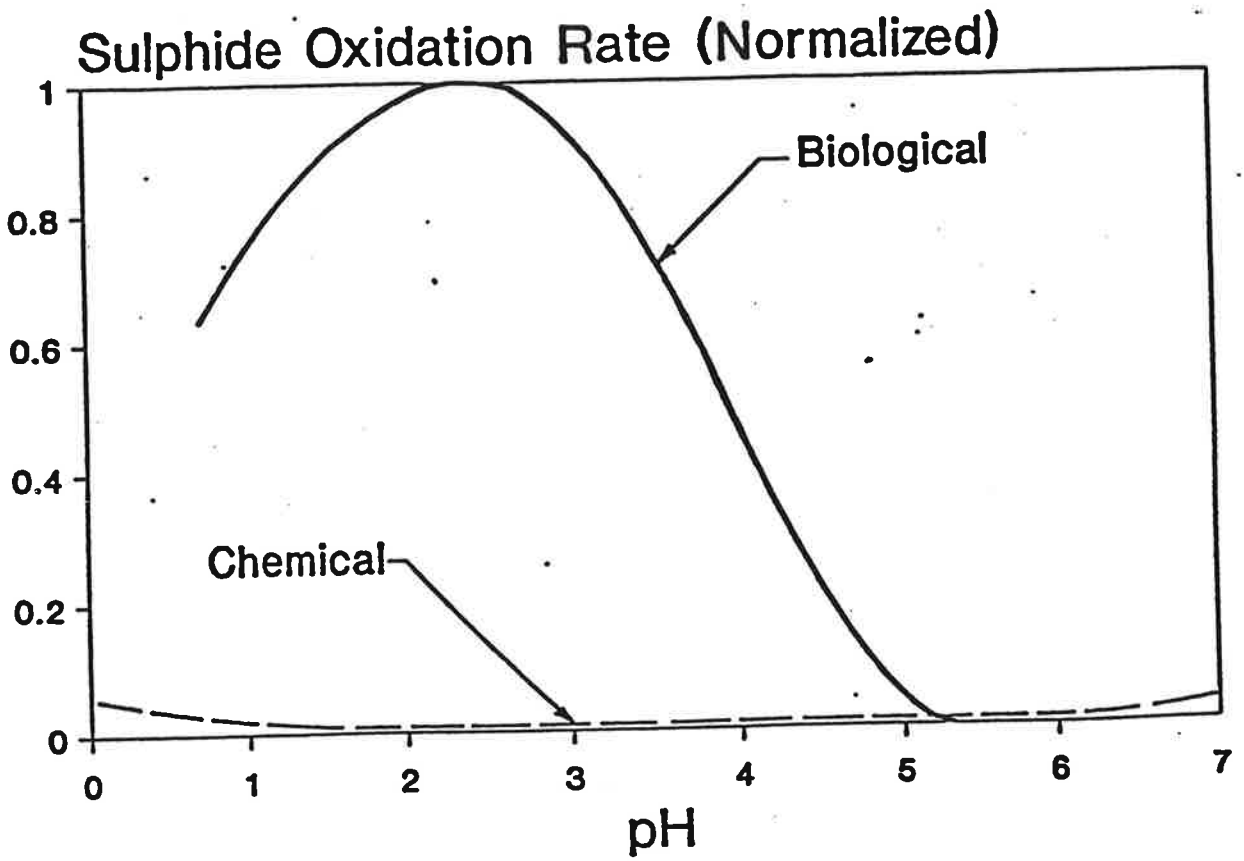

Figure 3.1: Sulphide oxidation as a function of pH following ref. 16.

which elevates acid of the water and thus lowers its pH.

(2) Provided the supply of oxygen in the environment is sufficient, ferrous iron oxidizes to ferric iron

$$Fe^{2+} + \frac{1}{4}O_2(s) + H^+(aq) \underset{k_{-2}}{\overset{k_2}{\rightleftharpoons}} Fe^{3+} + \frac{1}{2}H_2O. \tag{3.2}$$

(3) Ferric iron then precipitates as $Fe(OH)_3$ at pH values above 2.3 to 3.5

$$Fe^{3+} + 3H_2O \underset{k_{-3}}{\overset{k_3}{\rightleftharpoons}} Fe(OH)_3 + 3H^+ \tag{3.3}$$

resulting in the lowering of pH.

(4) Any remaining amount of Fe^{3+} can be used to oxidize additional pyrite from the reaction (1) providing a *feedback loop*

$$FeS_2 + 14Fe^{3+} + 8H_2O \xrightarrow{k_4} 15Fe^{2+} + 2SO_4^{2-}(aq) + 16H^+(aq). \tag{3.4}$$

This set of reactions (3.1), (3.2) and (3.3) can be graphically illustrated as shown in Figure 3.2[DARDTG v.1].

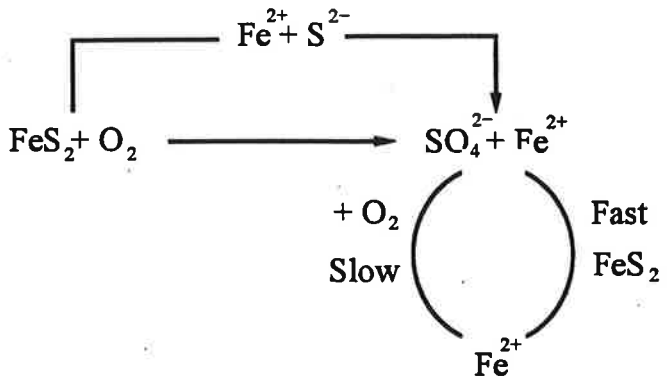

Figure 3.2: Graphical illustration of the combined reactions (3.1), (3.2) and (3.3).

A combination of the first three reactions gives acidic leachates according to

$$FeS_2 + \frac{15}{4}O_2 + \frac{7}{2}H_2O \rightarrow Fe(OH)_3 + 2SO_4^{2-} + 4H^+ \tag{3.5}$$

which applies mainly to low pH pyrite oxidation, while including all the reactions other than the third produces

$$FeS_2 + \frac{15}{8}O_2 + \frac{13}{2}Fe^{3+} + \frac{17}{4}H_2O \rightarrow \frac{15}{2}Fe^{2+} + 2SO_4^{2-} + \frac{17}{4}H^+ \tag{3.6}$$

which is schematically shown in the diagram above and applies to high pH pyrite oxidation.

Fig. 3.3 shows the above reactions as occurring in three distinct stages:

- Stage I (alkaline), mainly chemical oxidation occurs producing alkaline drainage with elevated sulphate and metals.

- Stage II (transitional).

- Stage III (acidic) results in elevated sulphate levels and acidity. Acidity here is a measure of accumulation of Fe^{2+}, $Fe(OH)^{2+}$, Al^{3+} and HSO_4^-. Unless neutralization processes take place at significant levels, there is a strong correlation between the amount of sulphates and acidity.

We have summarized the properties of the four constituent reactions in Table 3.1 below following the report of Otwinowski [Otwinowski (1993)]. Each reaction rate $k_i (i = 1, 2, 3, 4)$ is believed to be dependent on temperature through the Arrhenius relation

$$k_i = A_i \exp\left[\frac{E_i(T - T_o)}{RTT_o}\right] \tag{3.7}$$

where T is the temperature in degrees Kelvin, E_i is an activation energy, R is the gas constant and T_o is a characteristic temperature.

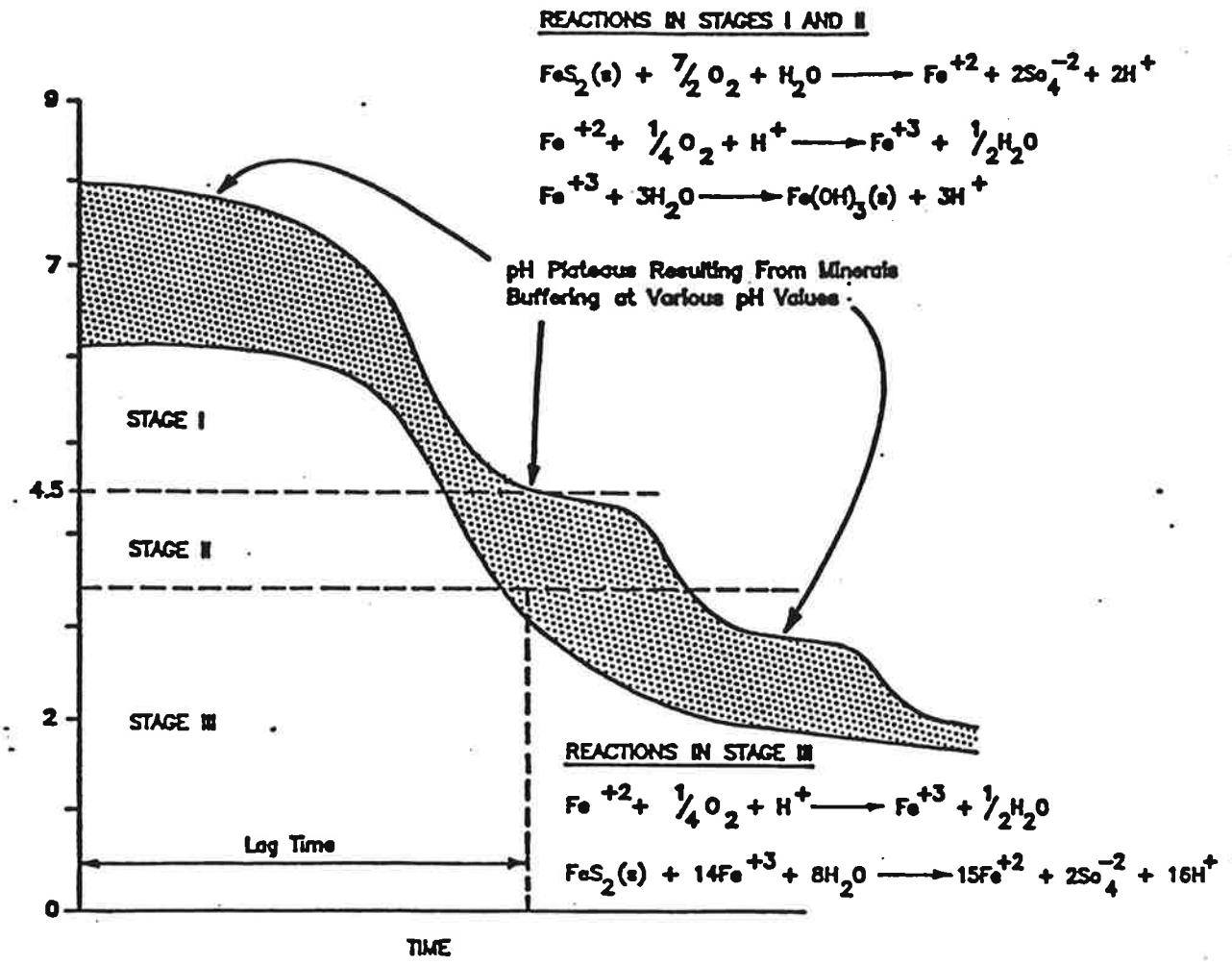

Figure 3.3: Stages in the formation of acid rock drainage following ref. 16.

3.3 Acid Neutralization

On the other hand, there exist several acid consuming minerals, such as calcite ($CaCO_3$) and gibbsite ($Al(OH_3)$) that neutralize the products of oxidation through the following types of reactions:

$$CaCO_3(s) + H^+ \rightarrow Ca^{2+}(aq) + HCO_3^-(aq) \tag{3.8}$$

or

$$CaCO_3(s) + 2H^+ \rightarrow Ca^{2+}(aq) + H_2CO_3^-(aq) \tag{3.9}$$

and

$$Al(OH)_3 + 3H^+ \rightarrow Al^{3+} + 3H_2O. \tag{3.10}$$

The balance between the two types of processes (acid production and acid neutralization) determines the net amount of acidity.

As was mentioned earlier, our interests lie in studying the kinetics of the chemical reactions discussed here and in the determination of the influence of both external conditions and internal composition on the overall rate of ARD. In the next section we derive

Reaction No.	Rate	Activation Energy	pH-dependence
(1)	$k_1 = 2.83 \times 10^{-9} cm^{-1/2} s^{-1}$ at $T = 30°$ C	$E_1 = 57 \pm 7.5$kJ/mol	pH independent up to pH=7.
(2)	depends on pH $k_{21} = 1.66 \times 10^{-9} atm^{-1} s^{-1}$ for $pH \leq 3.5$; $T_o = 25°C$ $k_{22} = 4.0 \times 10^{-6} M^{-1} atm^{-1} s^{-1}$ for $pH < 2$; $T_o = 30°C$ $k_{23} = 1.33 \times 10^{13} M^{-2} atm^{-1} s^{-1}$ for $pH > 4.5$; $T_o = 25°C$	$E_{21} = 74$ kJ/mol for $pH < 3.5$ $E_{22} = 85$ kJ/mol for $3.5 < pH < 5$ $E_{23} = 96$ kJ/mol for $pH > 5$	pH independent up to pH=3.5. first order w.r.t. OH^- for $3.5 < pH < 5$. second order w.r.t. OH^- for $pH > 5$.
(3)	-	-	strongly pH dependent
(4)	$k_4 = 3.03 \times 10^{-12} M cm^{-2} s^{-1}$ at $T_o = 30°$C.	$E_4 = 90$ kJ/mol.	complicated

Table 3.1: A summary of characteristic properties of the four reactions in eqs. (3.1)-(3.4) following Otwinowski (1993).

the equations governing the nonlinear chemical kinetics for both acid generation and acid neutralization processes. This will be followed by numerical modelling under a diverse range of conditions.

Section 4

Modelling and Its Results

In this section we set up the equations for the chemical kinetics of the AMD problem and then provide a host of numerical results obtained under different conditions. We analyze separately the two groups of reactions, i.e.: (a) acid production and (b) neutralization reactions. In the last subsection we deal with the issue of the modelling of chemical reactions occurring in porous media.

4.1 Acid Production (Homogeneous Medium)

The four reactions studied here are:

$$2FeS_2 + 7O_2 + 2H_2O \underset{k_{-1}}{\overset{k_1}{\rightleftharpoons}} 2Fe^{2+} + 4SO_4^{2-} + 2H^+ \tag{4.1}$$

$$4Fe^{2+} + O_2 + 4H^+ \underset{k_{-2}}{\overset{k_2}{\rightleftharpoons}} 4Fe^{3+} + 2H_2O \tag{4.2}$$

$$Fe^{3+} + 3H_2O \underset{k_{-3}}{\overset{k_3}{\rightleftharpoons}} Fe(OH)_3 + 3H^+ \tag{4.3}$$

$$FeS_2 + 14Fe^{3+} + 8H_2O \underset{k_{-4}}{\overset{k_4}{\rightleftharpoons}} 15Fe^{2+} + 2SO_4^{2-} + 16H^+. \tag{4.4}$$

For the sake of convenience we introduce the following notation for the concentrations of the chemical species present

$$X_1 \equiv [FeS_2]; \quad X_2 \equiv [O_2]; \quad X_3 \equiv [H_2O]; \quad X_4 \equiv [Fe^{2+}];$$
$$X_5 \equiv [SO_4^{2-}]; \quad X_6 \equiv [H^+]; \quad X_7 \equiv [Fe^{3+}]; \quad X_8 \equiv [Fe(OH)_3]$$

For all practical purposes the above reactions are not reversible due to the large free energy of reaction involved. Since our analysis did not become much more complicated by the inclusion of reverse reactions and we set out to investigate the most extreme role nonlinearity may play, we nonetheless performed several simulation with the presence of

reverse reactions. Based on the discussion provided in the previous section we set up the equations of chemical kinetics for these processes as follows:

$$\dot{X}_1 = -k_1 X_1^2 X_2^7 X_3^2 - k_4 X_1 X_7^{14} X_3^8 \tag{4.5}$$

$$\dot{X}_2 = -\frac{7}{2} k_1 X_1^2 X_2^7 X_3^2 - k_2 X_4^4 X_2 X_6^4 \tag{4.6}$$

$$\dot{X}_3 = -k_1 X_1^2 X_2^7 X_3^2 + 2k_2 X_4^4 X_2 X_6^4 - k_3 X_7 X_3^3 - 8k_4 X_1 X_7^{14} X_3^8 \tag{4.7}$$

$$\dot{X}_4 = k_1 X_1^2 X_2^7 X_3^2 - 4k_2 X_4^4 X_2 X_6^4 + 15k_4 X_1 X_7^{14} X_3^8 \tag{4.8}$$

$$\dot{X}_5 = 2k_1 X_1^2 X_2^7 X_3^2 + 2k_4 X_1 X_7^{14} X_3^8 \tag{4.9}$$

$$\dot{X}_6 = k_1 X_1^2 X_2^7 X_3^2 - 4k_2 X_4^4 X_2 X_6^4 + k_3 X_7 X_3^3 + 16k_4 X_1 X_7^{14} X_3^8 \tag{4.10}$$

$$\dot{X}_7 = 4k_2 X_4^4 X_2 X_6^4 - \frac{1}{3} k_3 X_7 X_3^3 - 14k_4 X_1 X_7^{14} X_3^8 \tag{4.11}$$

$$\dot{X}_8 = k_3 X_7 X_3^3 \tag{4.12}$$

Note that at this stage we have not included the possibility of either reverse reactions, or inflows into and outflows out of the system. The above equations automatically satisfy mass balance and we checked it numerically for all our solutions. We should make here an important qualification. The equations we derived above are only valid for elementary reactions. in reality, the stoichiometric coefficients imposed above can not be used a priori as the order of reactions for complex reactions. Hence, the order of reactions must be determined empirically. This effectively means that the approach we present here is simplified for the purpose of making the analysis easily tractable. It represents the most extreme scenario from the point of view of nonlinearity of the equations studied. However, at present we are unable to make the analysis more realistic for the lack of reliable experimental data.

Having no precise knowledge regarding the reaction rates we have run several trial computations with a range of test values of both initial values of concentrations and reaction rate magnitudes. Our findings are illustrated in Figs. 4.1–4.8. In Fig. 4.1–4.8 (and also further below) we have normalized the concentrations of all the chemical species $\{X_1, \ldots, X_8\}$ to be within the 0 to 1 range, 0 meaning complete depletion and 1 complete saturation. This has been dictated by expediency and simplicity. We do not have precise knowledge of the abundances and reaction rates but at this stage we were mainly interested in qualitative behavior. The time variable is also scaled and is represented in arbitrary units. However, in reality the time units will be those of the slowest reaction in the chain. Comparing with Figs. 5.1–5.4 we can make an educated guess and identify one time unit in our diagrams with approximately 10–15 days of real time. The initial points (ie. those at $t = 0$) were selected in several possible ways in order to examine various feasible situations. For example, it was commonly assumed that FeS_2, O_2 and H_2O are initially at their saturation levels while the remaining five species are, in the beginning, not present. As the reader may see from the figure captions, other possibilities were also considered. The reaction rates were all set at unity except for Fig. 4.4 where $k_2 = k_3 = 0.1$ (with very little change in the qualitative behavior). The numerical codes used in these simulations are very reliable and give consistant, reproducible results. We have a measure of confidence in our findings and intend to perform more computations with different input data in the future. As the reader may easily appreciate, the problem is not computational in nature, but rests with obtaining a reliable set of empirically-based input data.

We have studied the above equations under a number of different conditions as well. What emerges, however, can be summarized as a rather smooth and regular tendency of all the chemical species involved to reach their equilibrium concentrations. This is the case whether we change the initial concentrations or vary the reaction rates for the various reactions. Therefore, at this stage of modelling complete predictability of these processes seems virtually guaranteed and no hallmarks of chaos or irregularity have been found.

In the next step of our investigation we attempted to find out if the behavior of the system significantly changes when reverse reactions are allowed to take place. To this end we assumed that $k_{-2} \neq 0$ and $k_{-3} \neq 0$ leaving $k_{-1} = k_{-4} = 0$. The relevant equations are different and they now become

$$\dot{X}_1 = -k_1 X_1^2 X_2^7 X_3^2 - k_4 X_1 X_7^{14} X_3^8 \tag{4.13}$$

$$\dot{X}_2 = -\frac{7}{2} k_1 X_1^2 X_2^7 X_3^2 - k_2 X_4^4 X_2 X_6^4 + k_2 X_7^4 X_3^2 \tag{4.14}$$

$$\dot{X}_3 = -k_1 X_1^2 X_2^7 X_3^2 + 2k_2 X_4^4 X_2 X_6^4 - 3k_3 X_7 X_3^3 - 8k_7 X_1 X_7^{14} X_3^8 - 2k_2 X_7^4 X_3^2 + 3k_3 X_8 X_6^3 \tag{4.15}$$

$$\dot{X}_4 = k_1 X_1^2 X_2^7 X_3^2 - 4k_2 X_4^4 X_2 X_6^4 + 15k_4 X_1 X_7^1 4 X_3^8 + 4k_{-2} X_7^4 X_3^2 \tag{4.16}$$

$$\dot{X}_5 = 2k_1 X_1^2 X_2^7 X_3^2 + 2k_4 X_1 X_7^1 4 X_3^8 \tag{4.17}$$

$$\dot{X}_6 = k_1 X_1^2 X_2^7 X_3^2 - 4k_2 X_4^4 X_2 X_6^4 + 3k_3 X_7 X_3^3 + 16k_4 X_1 X_7^1 4 X_3^8 + 4k_{-2} X_7^4 X_3^2 - 3k_{-3} X_8 X_6^3 \tag{4.18}$$

$$\dot{X}_7 = 4k_2 X_4^4 X_2 X_6^4 - k_3 X_7 X_3^3 - 14k_4 X_1 X_7^1 4 X_3^8 - 4k_{-2} X_7^4 X_3^2 + k_{-3} X_8 X_6^3 \tag{4.19}$$

$$\dot{X}_8 = k_3 X_7 X_3^3 - k_{-3} X_8 X_6^3 \tag{4.20}$$

A sample result of our numerical simulation of this system is shown in Fig. 4.9 where we have exaggerated the effect somewhat by assuming that the reverse reaction rate is half of the forward rate. Nevertheless, what we obtained indicates a by and large smooth behavior and, again, a tendency towards equilibration . There is a short-lived period of non-monotonic behavior close to the beginning of the process but it rapidly gives way to the asymptotic trend towards equilibrium.

In the final stage of modelling the acid production processes we allow the presence of inflows into or outflows from the system. This applies to the abundances of water and oxygen. As a result, the only reactions that are affected by this change of prevailing conditions are

$$\dot{X}_2 = -\frac{7}{2} k_1 X_1^2 X_2^7 X_3^2 - k_2 X_4^4 X_2 X_6^4 + k_{-2} X_7^4 X_3^2 - f_2(X_2 - \bar{X}_2) \tag{4.21}$$

$$\dot{X}_3 = -k_1 X_1^2 X_2^7 X_3^2 + 2k_2 X_4^4 X_2 X_6^4 - 2k_{-2} X_7^4 X_3^2 - 3k_3 X_7 X_3^3 + 3k_{-3} X_8 X_6^3 - 8k_4 X_1 X_7^1 4 X_3^8 - f_2(X_3 - \bar{X}_3) \tag{4.22}$$

where f_2 and f_3 are the mean flow rates for oxygen and water, respectively, while $\bar{X}_2$ and $\bar{X}_3$ represent the equilibrium values of the oxygen and water concentrations, respectively.

What follows is a selection of modelling results for a variety of initial conditions, reaction rates and flow rates. Fig. 4.10 illustrates the effect of flow rates on the chemical kinetics. It is assumed here that no reverse reactions are present. Note again the smoothness and regularity of the resultant behavior.

In Figs. 4.11-4.18 we illustrate the behavior when both reverse reactions and flow rates are nonzero. The first group of diagrams shows the chemical kinetics for positive flow rates (Figs. 4.11-4.13) while the second group (Figs. 4.13-4.18) allows one or both of the flow rates to be negative.

To summarize our findings in this part we emphasize the very sensitive dependence of the chemical kinetics on the flow rates. This is evident for both positive and negative flow rates. In the former case, a drastic difference is clearly seen in the intermediate time range on going from Fig. 4.11 to Fig. 4.12 resulting from a change in the magnitudes of f_2 and f_3. Asymptotically, however, positive flow rates result in a long-range smooth relaxation towards equilibrium concentrations. On the other hand, when one or two flow rates become negative, this leads to the emergence of divergent behavior in the associa ted generation of a given species. Simultaneously, the irregular, non-monotonic region of behavior is substantially extended in time.

4.2 Acid Production (Porous Medium)

As discussed in subsection 2.2, the net result of porosity in the medium where chemical reactions take place is that the reaction rates become strongly time dependent. It was argued earlier in this report that to effectively account for the porosity aspect of the medium, the chemical reaction studied must be assumed to have reaction rates such that [Kopelman (1986)]

$$k_i = k_i^{\circ} t^{-1/3} \qquad (i = 1, 2, 3, 4). \tag{4.23}$$

In order to study this effect we repeated our numerical modelling with the above conditions built into the coupled equations for chemical kinetics. Our results are summarized in Figs. 4.19-4.22.

What emerges from the diagrams above is an even more sensitive dependence on the flow rates for these reactions in a porous medium as compared to a homogeneous medium. Regions of transient non-monotonic behavior are extended in the time domain and much of the regularity has been removed. Strictly speaking, the long-time behavior presented in Figs. 4.20–4.22 contradicts the assumptions built into the model since some of the concentrations involved exceed their saturation values of one. One can deal with this by either further rescaling or a change in the initial conditions or, finally, by restricting the time variable. It should also be added that all these diagrams involve inflow-outflow conditions and hence the total mass is not conserved within the system over time.

An interesting observation based on this set of simulations can be made that the prevelence of monotonic growth or depletion characteristic of homogeneous models is here destroyed by the assumption that the medium is porous. The fractality of the rock (see discussion in Sec. 5.3) implies time-dependent reaction rates which lead to often non-monotonic chemical kinetics. It appears obvious, however, in view of earlier remarks that the scaling laws such as eq. (4.23) should have validity over a limited range of time, or conversely should be tempered by saturation factors.

4.3 Acid Neutralization Reactions

The main acid neutralization reactions are

$$CaCO_3 + H^+ \xrightarrow{K_1} Ca^{2+} + HCO_3^- \tag{4.24}$$

$$CaCO_3 + 2H^+ \xrightarrow{K_2} Ca^{2+} + H_2CO_3 \tag{4.25}$$

$$Al(OH)_3 + 3H^+ \xrightarrow{K_3} Al^{3+} + 3H_2O \tag{4.26}$$

$$\tag{4.27}$$

where K_1, K_2 and K_3 are the associated reaction rates. For simplicity, we have introduced the following symbols for the concentrations of the chemical species present:

$Y_1 \equiv [CaCO_3]$; $Y_2 \equiv [H^+]$; $Y_3 \equiv [Ca^{2+}]$; $Y_4 \equiv [HCO_3^-]$;
$Y_5 \equiv [H_2CO_3]$; $Y_6 \equiv [Al(OH)_3]$; $Y_7 \equiv [Al^{3+}]$; $Y_8 \equiv [H_2O]$

Using the same technique as in the preceding subsections we derive the kinetic equations for acid neutralization as

$$\dot{Y}_1 = -K_1Y_1Y_2 - K_2Y_1Y_2^2 \tag{4.28}$$

$$\dot{Y}_2 = -K_1Y_1Y_2 - 2K_2Y_1Y_2^2 - 3K_3Y_6Y_2^3 \tag{4.29}$$

$$\dot{Y}_3 = K_1Y_1Y_2 + K_2Y_1Y_2^2 \tag{4.30}$$

$$\dot{Y}_4 = K_1Y_1Y_2 \tag{4.31}$$

$$\dot{Y}_5 = K_2Y_1Y_2^2 \tag{4.32}$$

$$\dot{Y}_6 = -K_3Y_6Y_2^3 \tag{4.33}$$

$$\dot{Y}_7 = K_3Y_6Y_2^3 \tag{4.34}$$

$$\dot{Y}_8 = 2K_3Y_6Y_2^3 \tag{4.35}$$

This system is much simpler than the one for acid production and the order of nonlinearities is also significantly reduced. In fact, due to their structure, the equations on Y_3, Y_4, Y_5 and Y_7 are effectively decoupled from the remaining three and the dynamics is governed by the equations on Y_1, Y_2 and Y_6; the other four concentrations are solely determined by the results from the interplay between Y_1, Y_2 and Y_6. Not surprisingly, our numerical modelling of the acid neutralization reactions produced a very smooth and predictable behavior. This is illustrated on a sample result given in Fig. 4.23. We see that all the species concentrations follow monotonic curves to their equilibrium values. We conclude that the process of acid neutralization should be primarily determined by the abundance of $CaCO_3, H^+$ and the equilibrium reaction rates. No indications of nonlinear stochastic or chaotic behavior have been found and no challenges to the problem of predictability seem to be offered by this set of reactions. This is, of course, in contrast to the acid production reactions discussed above where a substantial amount of unpredictability exists due primarily to the two factors: (a) porosity of the medium and (b) flow rates of oxygen and water. Note that acid neutralization reactions do not seem to be dynamically coupled to the reactions of acid production. It is probably safe to assume that pH oscillations that can be observed just prior to acid generation are a result of this setup. Thus, such oscillations could be considered a good predictor of the onset of AMD process.

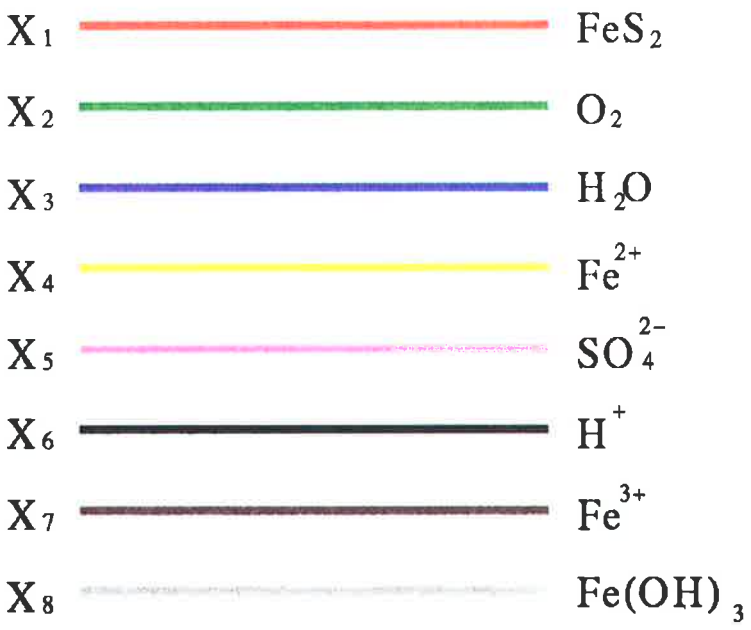

Color Legend for Figures 4.1–4.22.

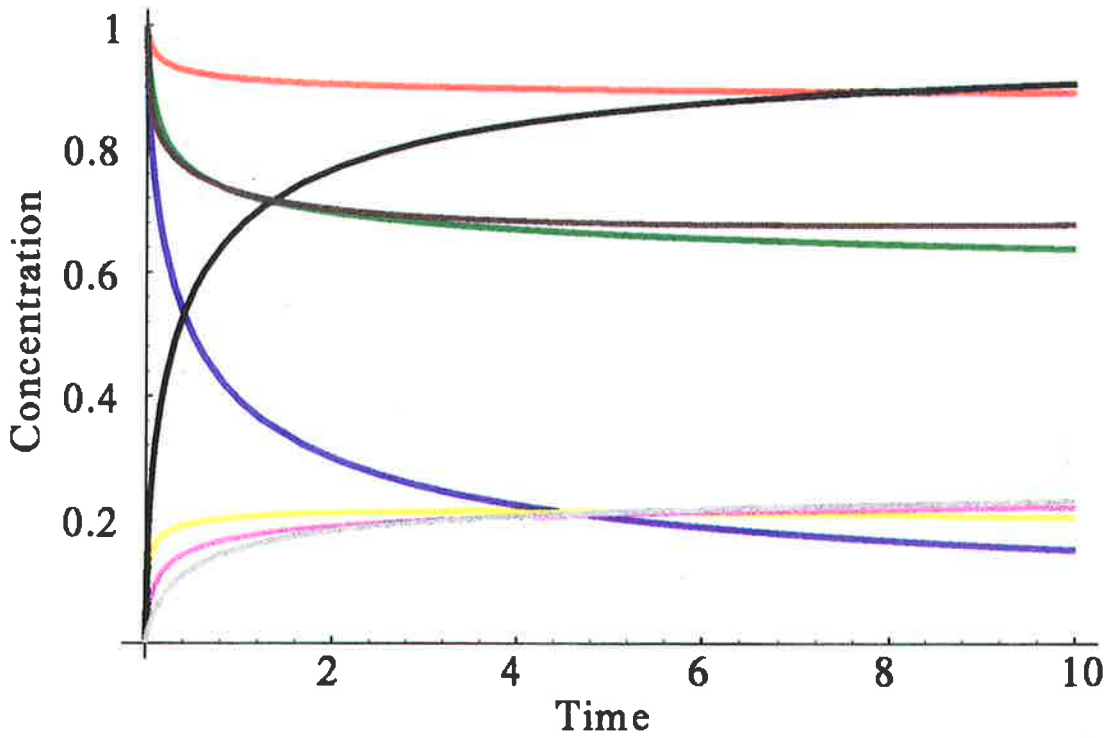

Figure 4.1: Chemical kinetics of the acid production reactions assuming: $X_1(0) = X_2(0) = X_3(0) = X_7(0) = 1, X_4(0) = X_5(0) = X_6(0) = X_8(0) = 0$ and $k_1 = k_2 = k_3 = k_4 = 1$. No inflow-outflow conditions and no reverse reactions are present.

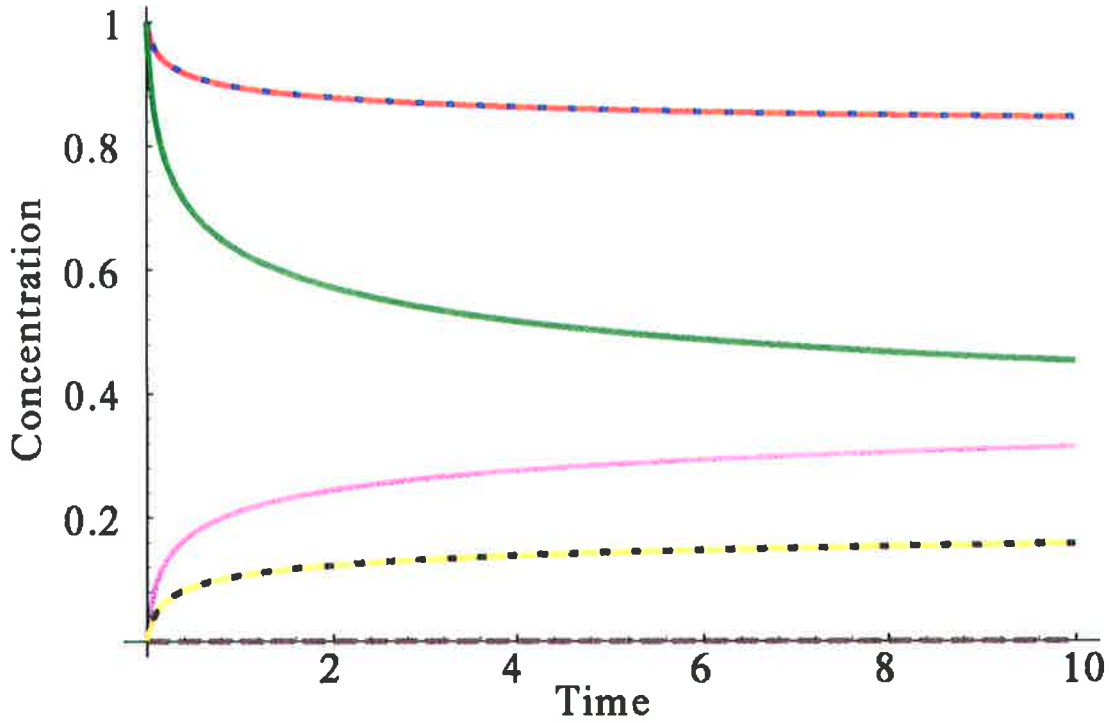

Figure 4.4: Chemical kinetics of the acid production reactions assuming: $X_1(0) = X_2(0) = X_3(0) = 0, X_4(0) = X_5(0) = X_6(0) = X_7(0) = X_8(0) = 0$ and $k_1 = k_4 = 1.0, k_2 = k_3 = 0.1$. No inflow-outflow conditions and no reverse reactions are present.

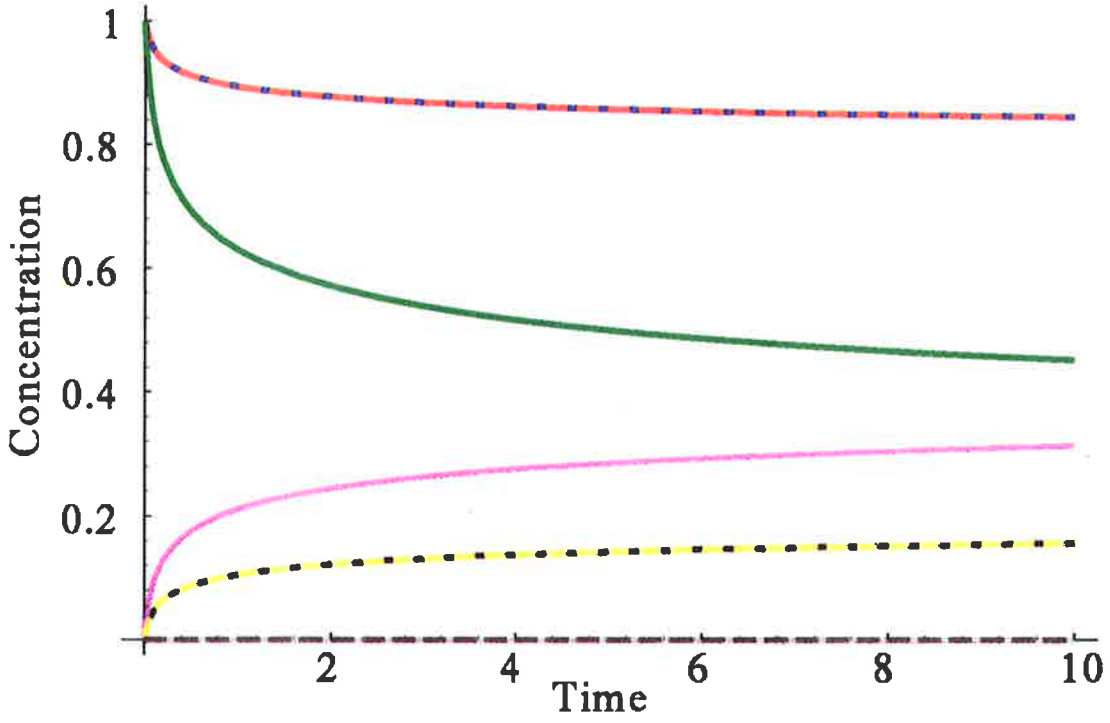

Figure 4.5: Chemical kinetics of the acid production reactions assuming: $X_1(0) = X_2(0) = X_3(0) = 1, X_4(0) = X_5(0) = \ldots = X_8(0) = 0$ and $k_1 = k_2 = k_3 = k_4 = 1$. No inflow-outflow conditions and no reverse reactions are present.

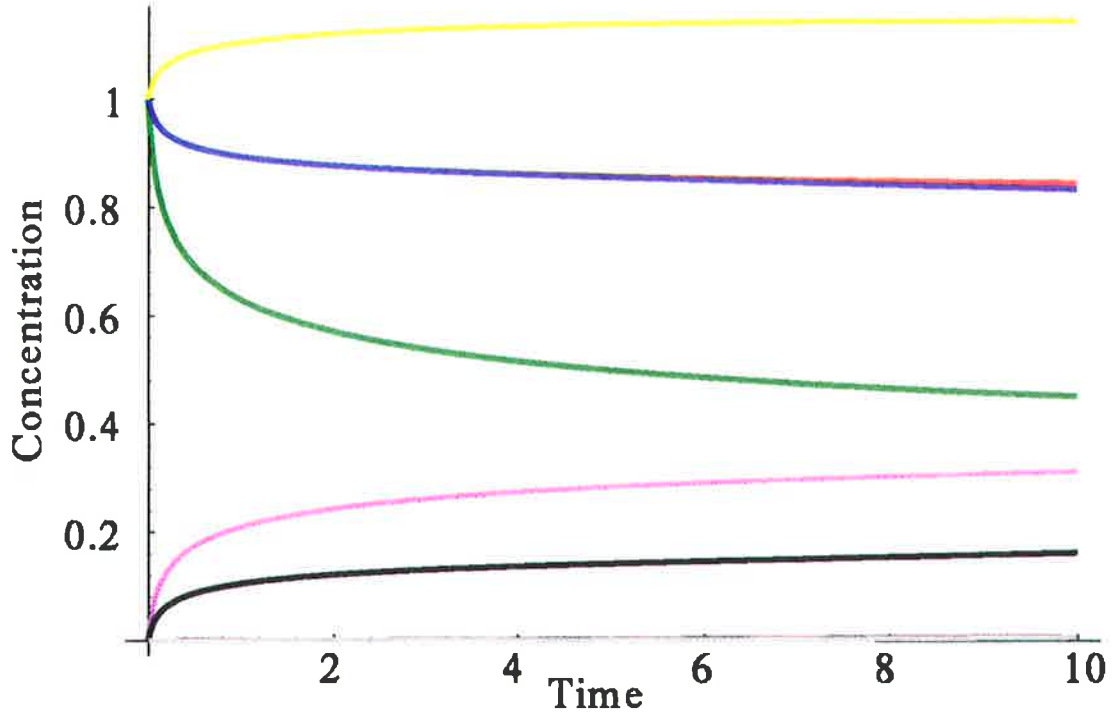

Figure 4.6: Chemical kinetics of the acid production reactions assuming: $X_1(0) = X_2(0) = X_3(0) = X_4(0) = 1, X_5(0) = X_6(0) = X_7(0) = X_8(0) = 0$ and $k_1 = k_2 = k_3 = k_4 = 1$. No inflow-outflow conditions and no reverse reactions are present.

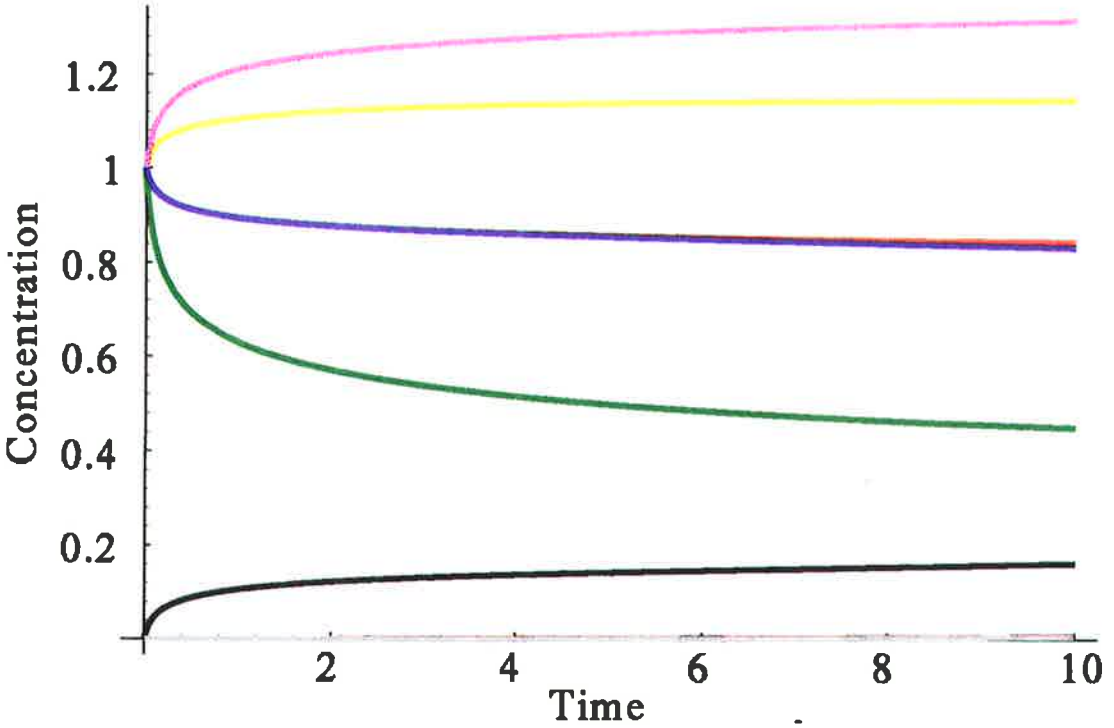

Figure 4.7: Chemical kinetics of the acid production reactions assuming: $X_1(0) = X_2(0) = X_3(0) = X_4(0) = X_5(0) = 1, X_6(0) = X_7(0) = X_8(0) = 0$ and $k_1 = k_2 = k_3 = k_4 = 1$. No inflow-outflow conditions and no reverse reactions are present.

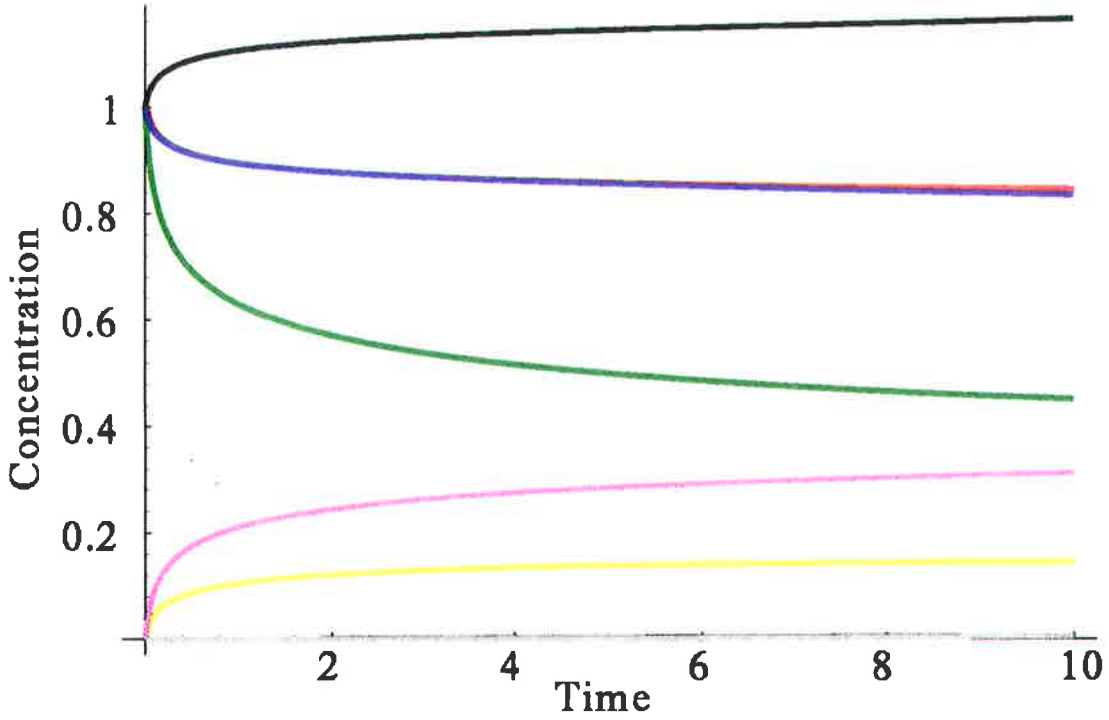

Figure 4.8: Chemical kinetics of the acid production reactions assuming: $X_1(0) = X_2(0) = X_3(0) = X_6(0) = 1, X_4(0) = X_5(0) = X_7(0) = X_8(0) = 0$ and $k_1 = k_2 = k_3 = k_4 = 1$. No inflow-outflow conditions and no reverse reactions are present.

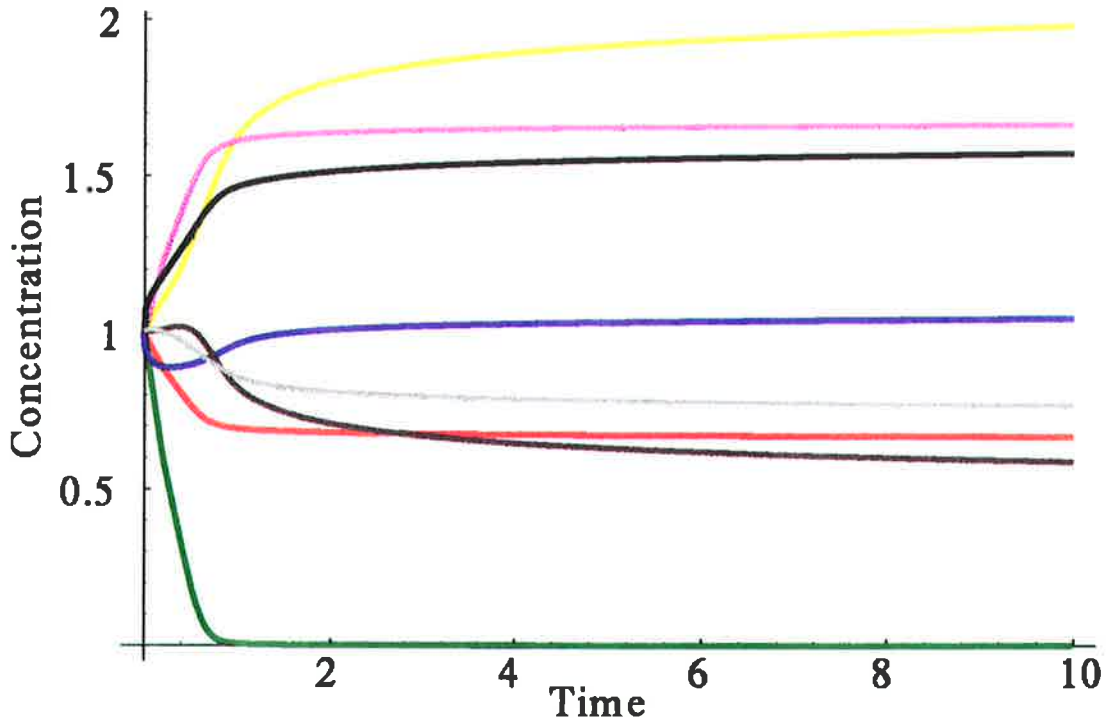

Figure 4.9: Chemical kinetics of the acid production reactions assuming that $X_1(0) = \ldots = X_8(0) = 1, k_1 = k_2 = k_3 = k_4 = 1$ and $k_{-2} = k_{-3} = 0.5$.

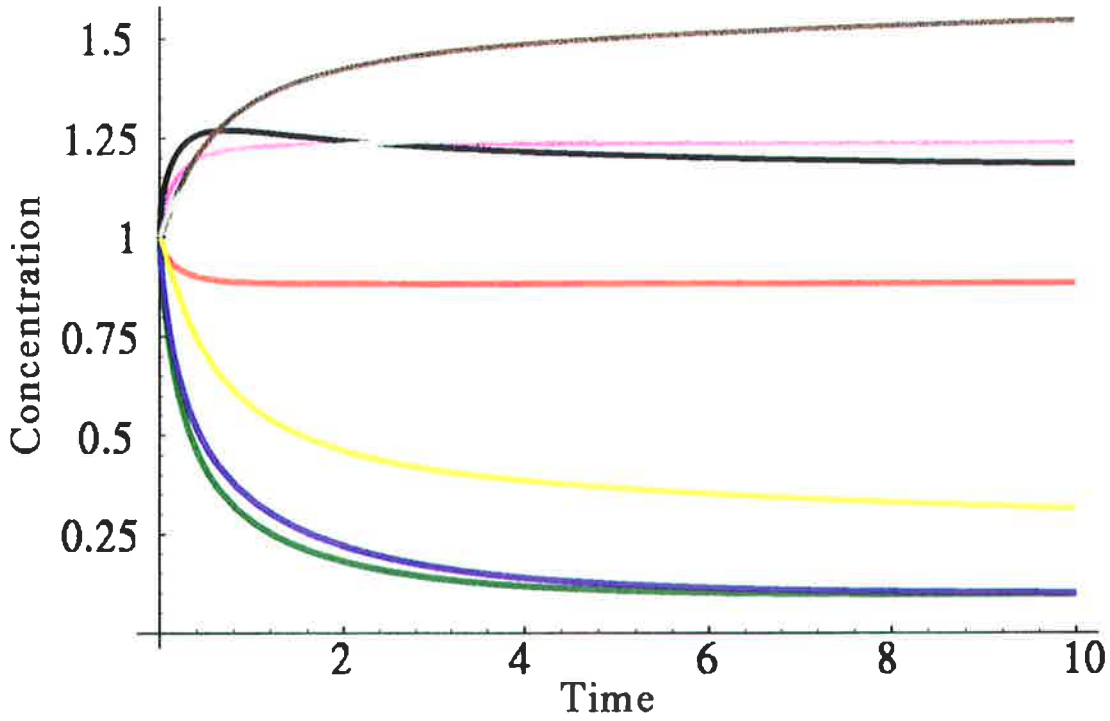

Figure 4.10: Chemical kinetics for the acid producing reactions assuming that $X_1(0) = \ldots = X_8(0) = 1, k_1 = k_2 = k_3 = k_4 = 1$, no reverse reactions are present, the flow rates are $f_2 = f_3 = 0.5$ and the equilibrium concentrations are $\bar{X}_2 = \bar{X}_3 = 0.1$.

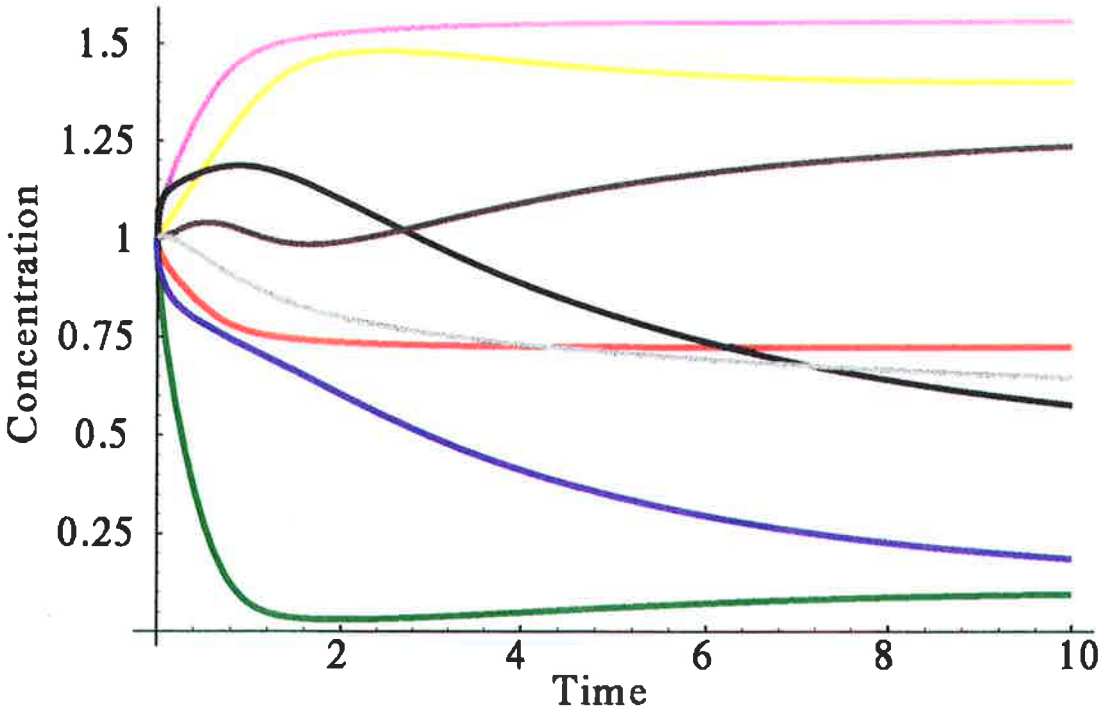

Figure 4.11: Chemical kinetics for the acid producing reactions assuming that $X_1(0) = \ldots = X_8(0) = 1$, $k_1 = k_2 = k_3 = k_4 = 1$, $k_{-2} = k_{-3} = f_2 = f_3 = 0.5$ and $\bar{X}_2 = \bar{X}_3 = 0.1$.

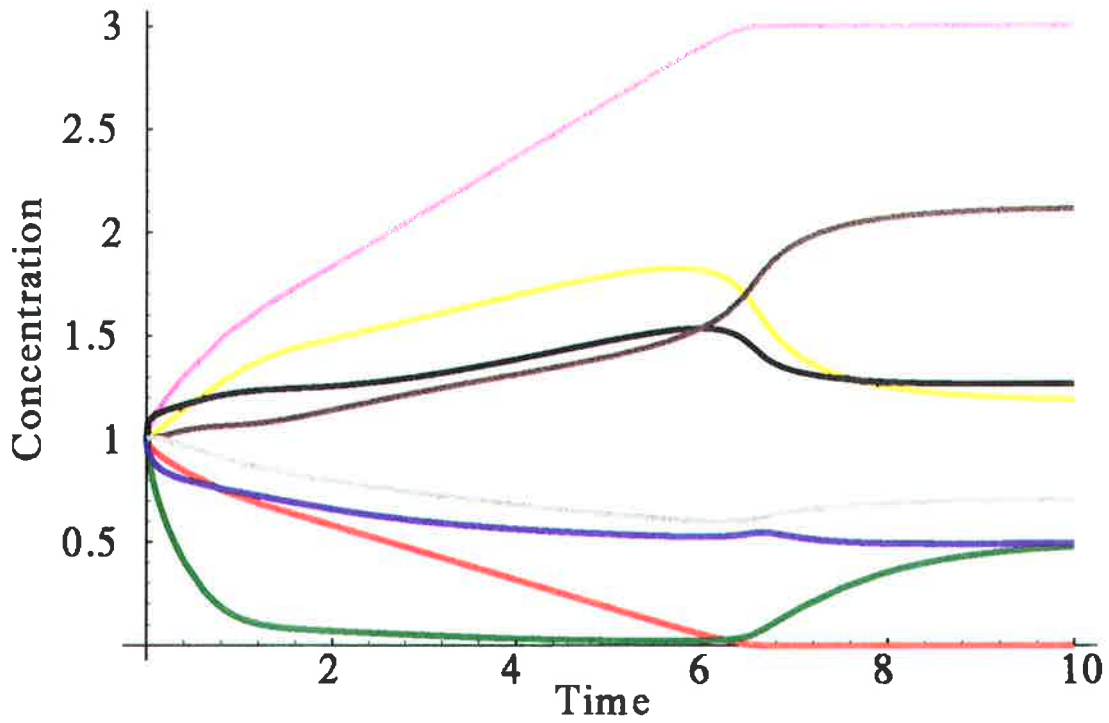

Figure 4.12: Chemical kinetics for the acid producing reactions assuming that $X_1(0) = \ldots = X_8(0) = 1$, $k_1 = k_2 = k_3 = k_4 = 1$, $k_{-2} = k_{-3} = 0.5$, $f_2 = f_3 = 1.0$ and $\bar{X}_2 = \bar{X}_3 = 0.5$.

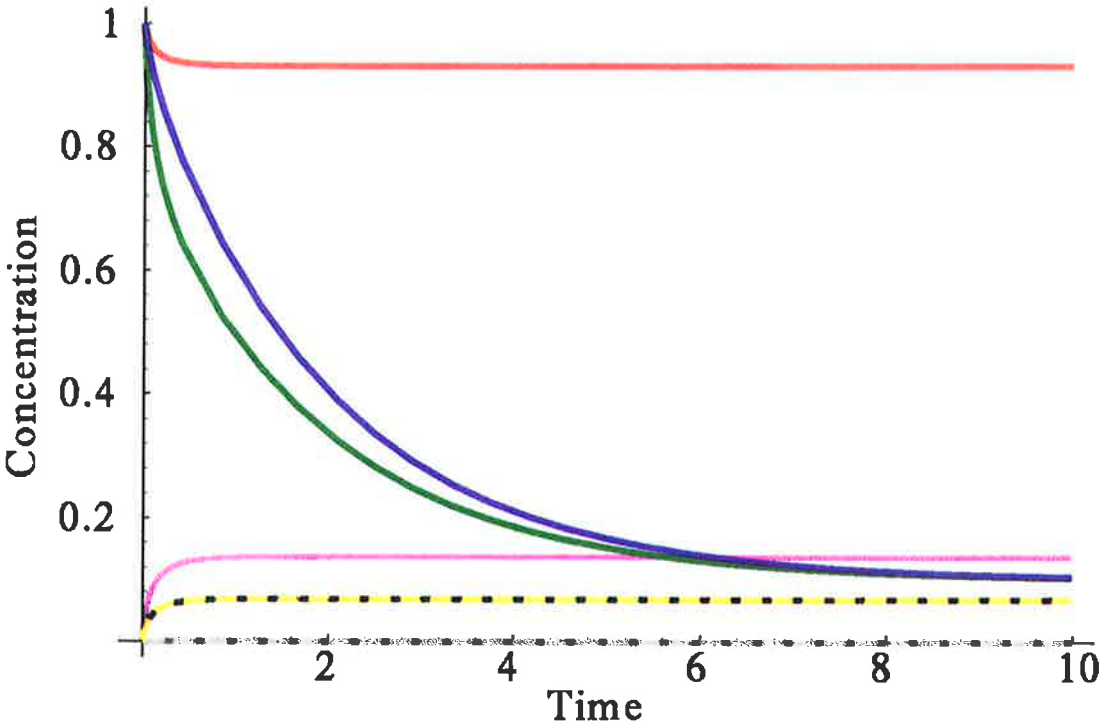

Figure 4.13: Chemical kinetics for the acid producing reactions assuming that $X_1(0) = X_2(0) = X_3(0) = 1$, $X_4(0) = \ldots = X_8(0) = 0$, $k_1 = k_2 = k_3 = k_4 = 1$, $k_{-2} = k_{-3} = f_2 = f_3 = 0.5$ and $\bar{X}_2 = \bar{X}_3 = 0.1$.

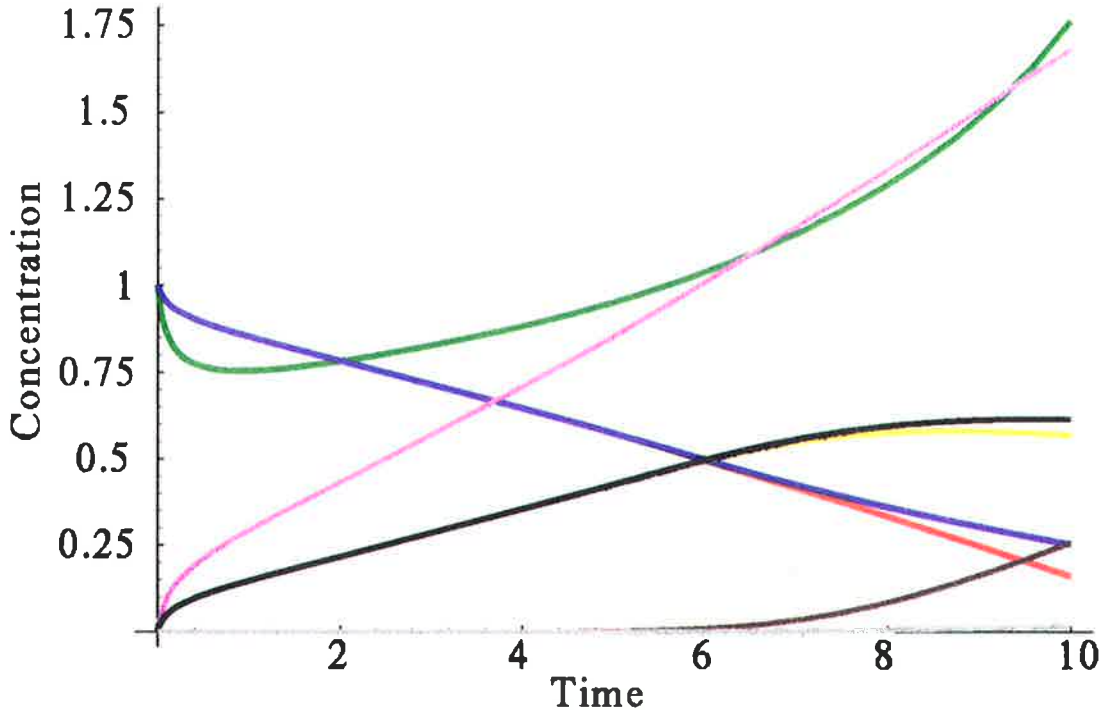

Figure 4.14: Chemical kinetics for the acid producing reactions assuming that $X_1(0) = X_2(0) = X_3(0) = 1$, $X_4(0) = \ldots = X_8(0) = 0$, $k_1 = k_2 = k_3 = k_4 = 1$, $k_{-2} = k_{-3} = 0.5$, $f_2 = -0.4$, $f_3 = 0$ and $\bar{X}_2 = \bar{X}_3 = 0.1$.

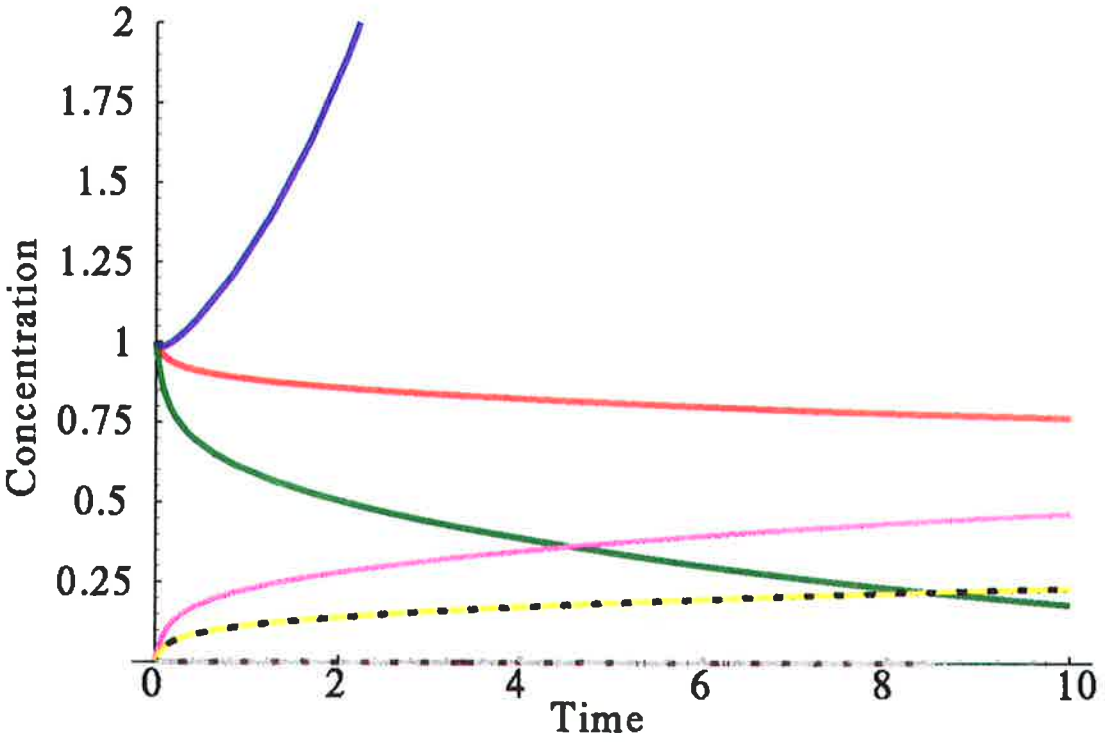

Figure 4.15: Chemical kinetics for the acid producing reactions assuming that $X_1(0) = X_2(0) = X_3(0) = 1$, $X_4(0) = \ldots = X_8(0) = 0$, $k_1 = k_2 = k_3 = k_4 = 1$, $k_{-2} = k_{-3} = 0.5$, $f_2 = 0; f_3 = -0.4$ and $\bar{X}_2 = \bar{X}_3 = 0.1$.

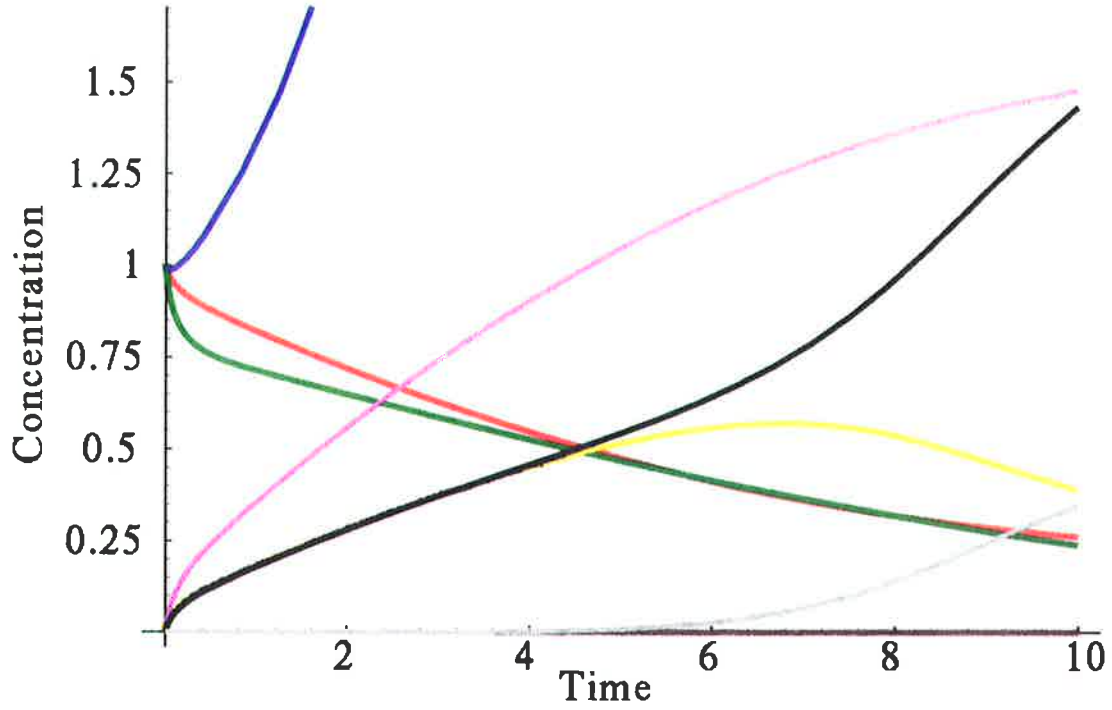

Figure 4.16: Chemical kinetics for the acid producing reactions assuming that $X_1(0) = X_2(0) = X_3(0) = 1$, $X_4(0) = \ldots = X_8(0) = 0$, $k_1 = k_2 = k_3 = k_4 = 1$, $k_{-2} = k_{-3} = 0.5$, $f_2 = f_3 = -0.5$ and $\bar{X}_2 = \bar{X}_3 = 0.1$.

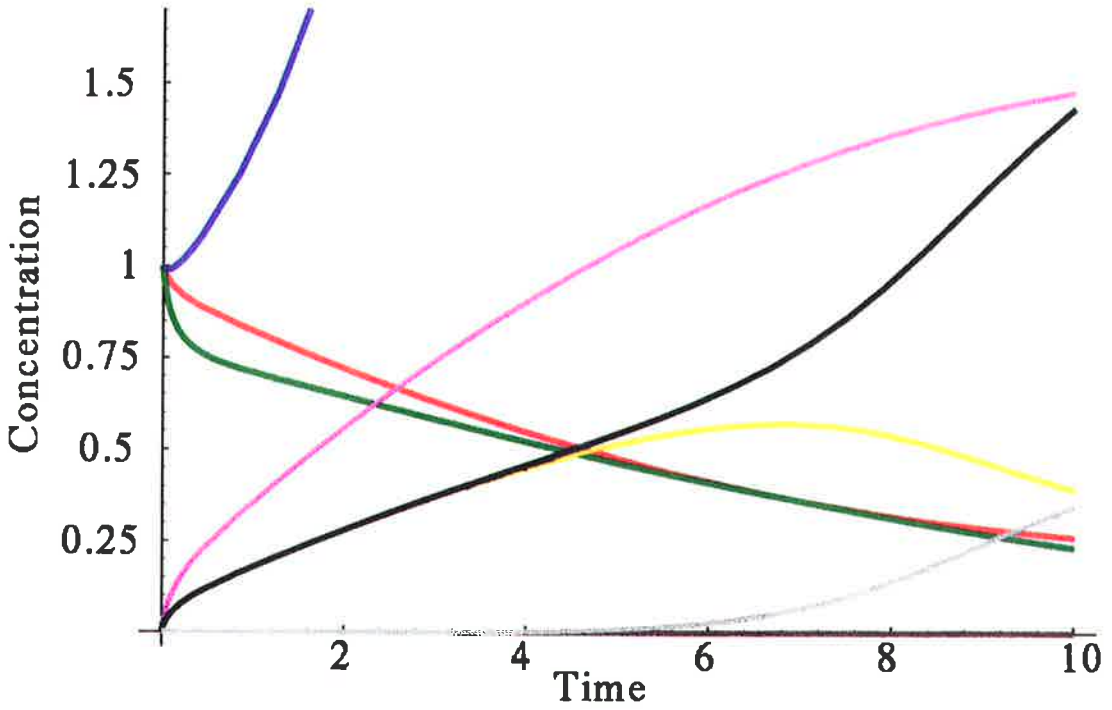

Figure 4.17: Chemical kinetics for the acid producing reactions assuming that $X_1(0) = X_2(0) = X_3(0) = 1$, $X_4(0) = \ldots = X_8(0) = 0$, $k_1 = k_2 = k_3 = k_4 = 1$, $k_{-2} = k_{-3} = 0$, $f_2 = f_3 = -0.5$ and $\bar{X}_2 = \bar{X}_3 = 0.1$.

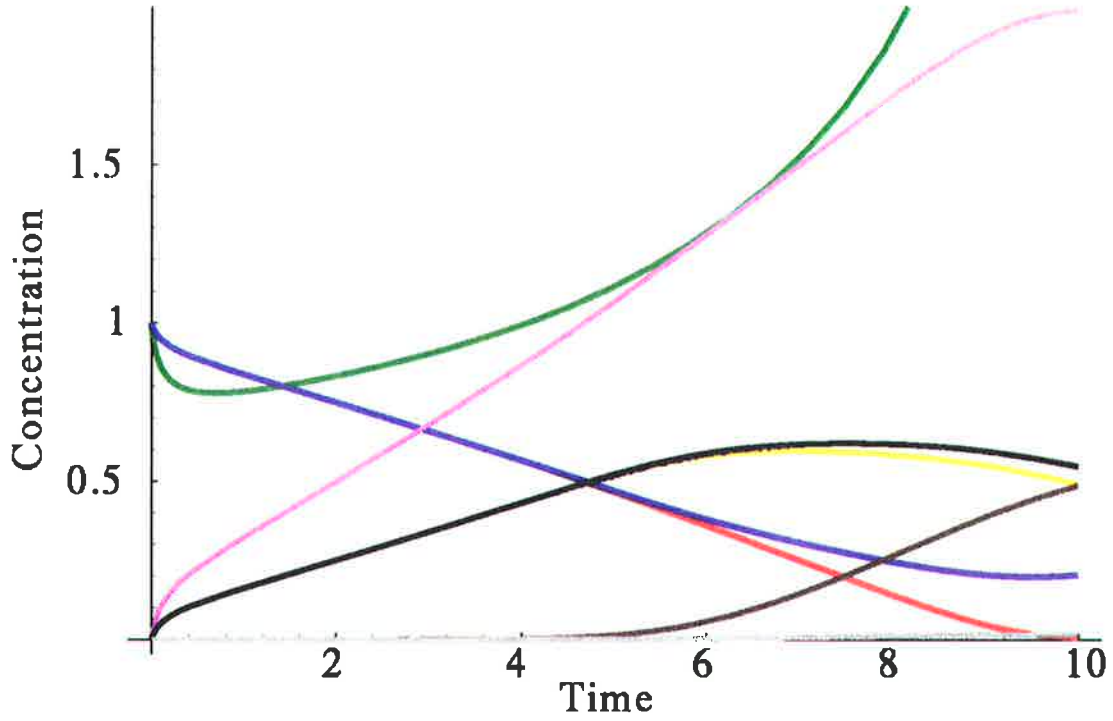

Figure 4.18: Chemical kinetics for the acid producing reactions assuming that $X_1(0) = X_2(0) = X_3(0) = 1$, $X_4(0) = \ldots = X_8(0) = 0$, $k_1 = k_2 = k_3 = k_4 = 1$, $k_{-2} = k_{-3} = 0$, $f_2 = -0.5$, and $f_3 = 0$ and $\bar{X}_2 = \bar{X}_3 = 0.1$.

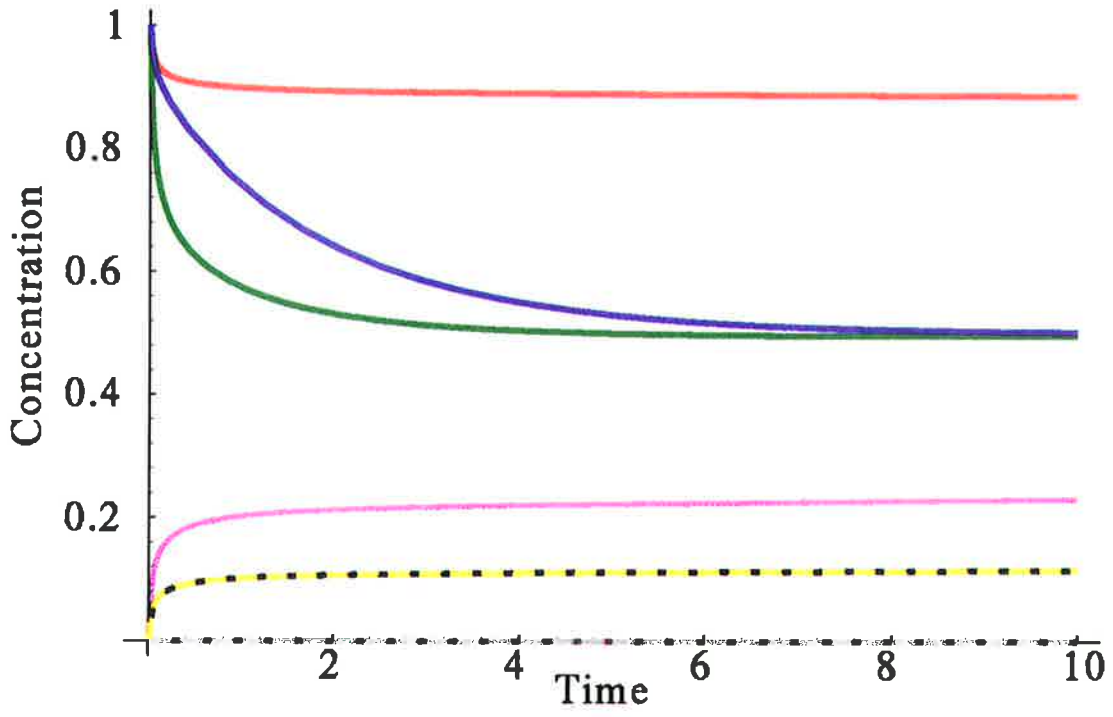

Figure 4.19: Chemical kinetics for the acid producing reactions in a porous medium with the assumption that $X_1(0) = X_2(0) = X_3(0) = 1, X_4(0) = \ldots = X_8(0) = 0, f_2 = f_3 = 0.5$ and $\bar{X}_2 = \bar{X}_3 = 0.5$.

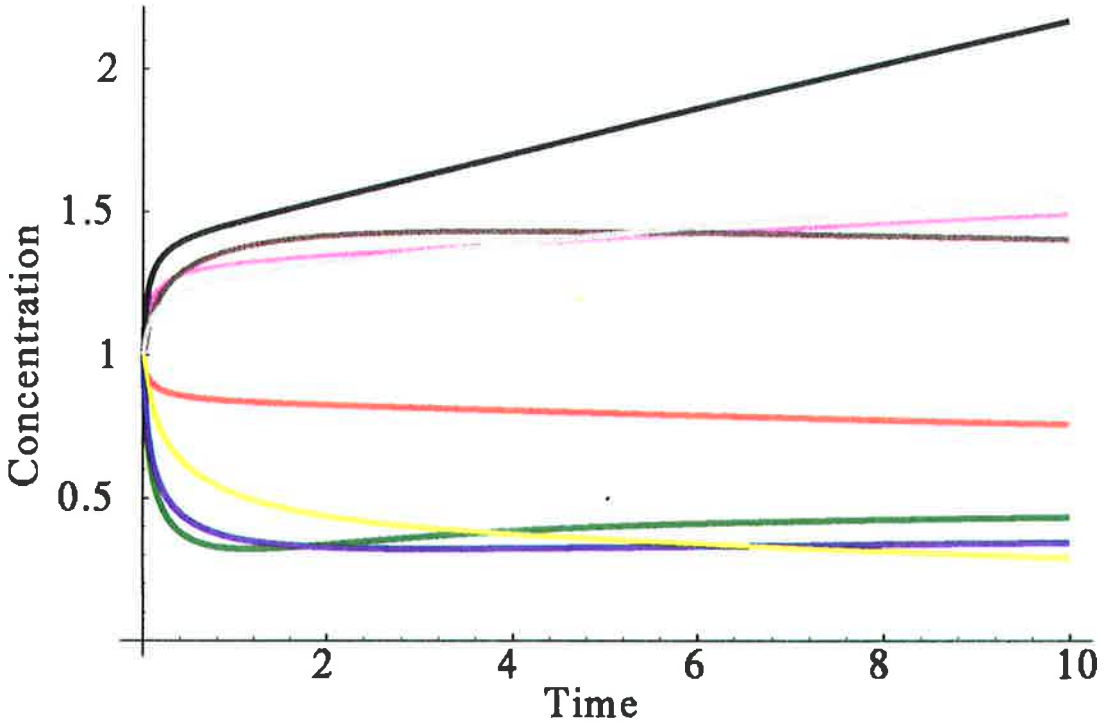

Figure 4.20: Chemical kinetics for the acid producing reactions in a porous medium with the assumption that $X_1(0) = \ldots = X_8(0) = 1, f_2 = f_3 = 0.5$ and $\bar{X}_2 = \bar{X}_3 = 0.5$.

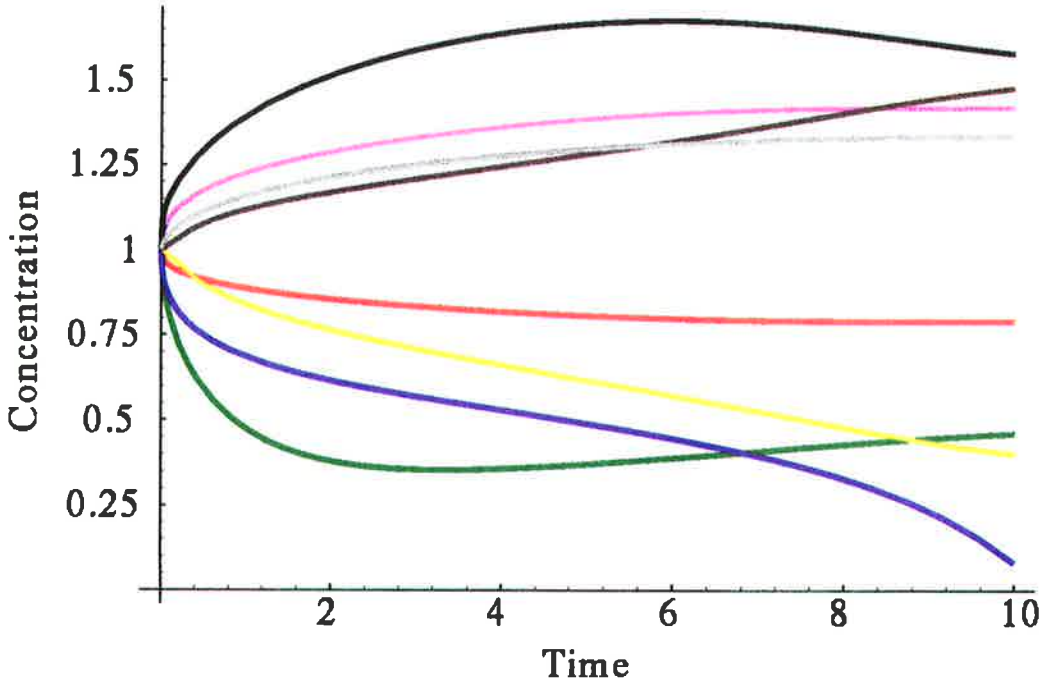

Figure 4.21: Chemical kinetics for the acid producing reactions in a porous medium with the assumption that $X_1(0) = \ldots = X_8(0) = 1, f_2 = 0.5, f_3 = -0.5$ and $\bar{X}_2 = \bar{X}_3 = 0.5$.

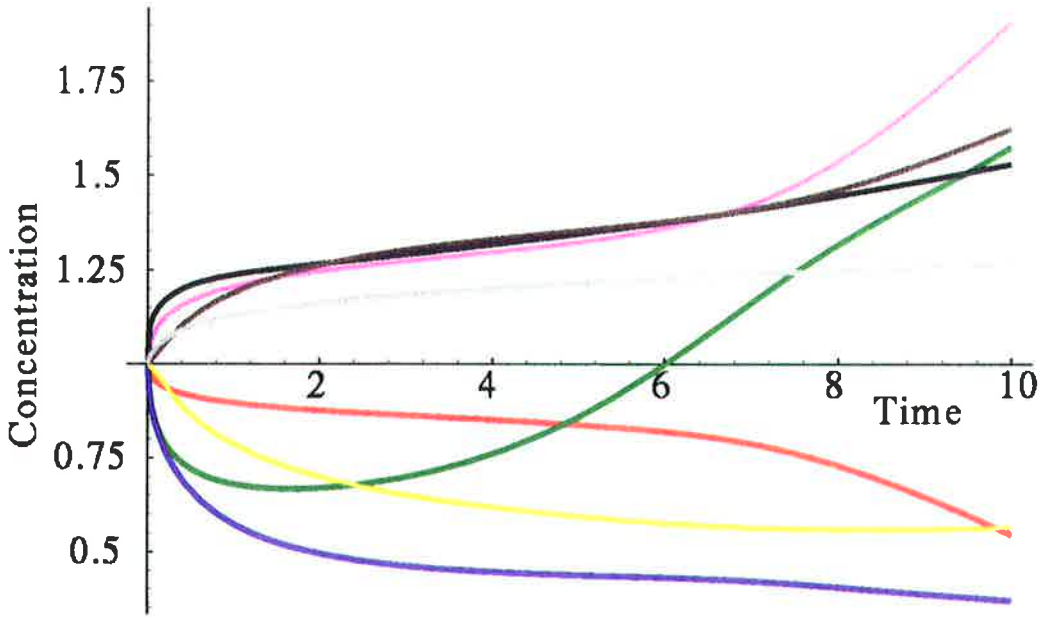

Figure 4.22: Chemical kinetics for the acid producing reactions in a porous medium with the assumption that $X_1(0) = \ldots = X_8(0) = 1, f_2 = -0.5, f_3 = 0.5$ and $\bar{X}_2 = \bar{X}_3 = 0.5$.

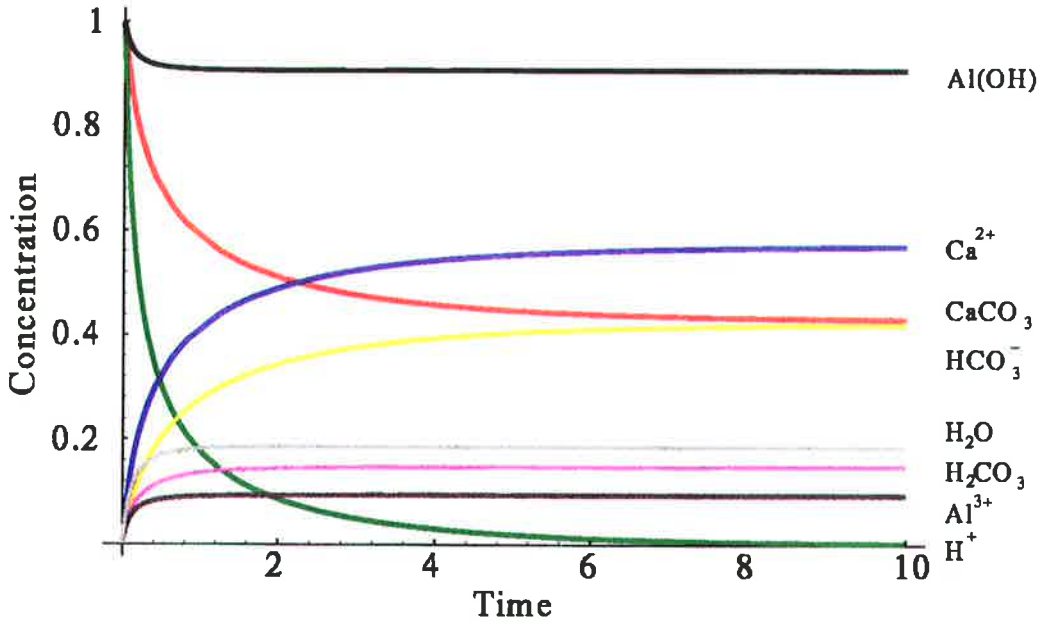

Figure 4.23: Chemical kinetics of the acid neutralization process where we have assumed that $Y_1(0) = Y_2(0) = Y_6(0) = 1, Y_3(0) = Y_4(0) = Y_5(0) = Y_7(0) = Y_8(0) = 0$, and that $K_1 = K_2 = K_3 = 1$.

Section 5

Discussion and Future Outlook

5.1 Summary and Conclusion

The present report has outlined the activity that has been undertaken within the framework of the above project.

First of all, a very extensive literature survey encompassing both geochemical analyses regarding the acid mine drainage problem and the relevant aspects of nonlinear chemical kinetics has been carried out. We have found detailed analyses regarding the primary chemical reactions involved in acid production. Qualitative aspects of chemical kinetics, such as which reactions are slow and which ones are fast can be readily found in the literature. Detailed characteristics in terms of activation energies and reaction rates were independently described by Dr. M. Otwinowski who submitted a parallel report.

In terms of nonlinear chemical kinetics we now have all the required information needed to solve the problem at hand. Several factors emerged as important theoretical considerations which were included in the numerical work described above. These are: (i) inflow-outflow ratios for water which will be strongly correlated with the porosity of the rock and seasonal variations such as rainfall, (ii) porosity of the medium, in contrast to the rather crude assumption about its homogeneity has been included in our model. Moreover, the inclusion of uncatalyzed reactions may be of importance in modelling, . We found that the effect of medium's porosity and size distribution of the rock can be accounted for by introducing time-dependent reaction rates. The time dependence required takes the form of power laws with exponents that are functions of the fractal dimension. The latter, in turn, is a characteristic quantity defining the structure of the rock and must be determined experimentally first (see Sec. 5.3).

The second stage of our work consisted in analyzing in detail the chemical kinetics in the AMD problem. We have set up the kinetic equations for the concentrations of the compounds involved. Two groups of equations have been investigated separately. In the acid production stage we found 8 coupled differential equations (highly nonlinear) for the concentrations of: $FeS_2, O_2, H_2O, Fe^{2+}, SO_4^{2-}, H^+, Fe^{3+}$ and $Fe(OH)_3$ and describing their time evolution. However, the last equation for $Fe(OH)_3$ is effectively decoupled from the rest making the system consist of 7 first-order ordinary differential equations. One of the results of this stage of chemical activity enters into the second stage, i.e. acid neutralization which is, otherwise, independent of the previous process. The acid neutralization stage involves 7 different concentrations, i.e.: $CaCO_3, H^+, Ca^{2+}, HCO_4^-, H_2CO_3, Al(OH)_3$ and Al^{3+}. The seven kinetic equations we

have set up are also nonlinear but this time the problem is substantially reduced as four of the equations decouple from the rest. Thus, we obtained just 3 coupled equations. This part of the project has been completed by building mass balance into the equations, carrying out dimensional analysis to maximally simplify the mathematical problem at hand and looking for steady states. No interesting steady-state solutions appear to exist other than complete depletions of reactants.

The third part of the problem has been to set up the numerical machinery at our disposal. With the newly acquired Next Work Station (including a laser printer) and the great time involvement of the students MLAN and DS, the required numerical code has been written and tested and many results obtained. Our results can be summarized as follows. Although the kinetic equations derived are highly nonlinear, no hallmarks of bifurcations or chaotic dynamics were found thus far. This would indicate the question of predictability is perhaps not as complicated as it could at first appear. However, we have also detected the presence of complex, non-monotonic behavior of the concentrations of the chemical species involved under special circumstances. This irregular behavior seems to be mainly affected by two factors:

(i) the porosity of the medium

(ii) the presence of non-zero flow rates of oxygen and water.

Thus, depending on the physical structure of the waste rock, specifically depending on the level of its inhomogeneity, the production of acid may follow a different course, being more regular in time for a more homogeneous medium than in a fractal-like distribution of waste rocks. Moreover, the flow rates of oxygen and water affect the reactions very significantly and they are certainly related to both climatic changes (rainfall, humidity) as well as the waste rock shape and structure, especially vis a vis the exposure to oxygen. Support of this conclusion can be found in the work of Doepker and Drake [Doepker et al.(1991)] where significantly different effects of leaching have been obtained between air-exposed and water-submerged tailings. Similarly, Steffen, Robertson and Kirsten[RPWQM Rep. No. 195201] show a marked difference in the production of SO_4 between flooded and unflooded test samples.

In numerous cases sulphate production kinetics exhibits a smooth, relaxation-type behavior with time. Test results shown by Steffen, Robertson and Kirtsten [RPWQM Rep. No. 195201], Denholm and Hallan [Denholm (1991)], Bradham and Caruccio [Bradham et al.] and Fergusen and Morin [Ferguson et al.] all indicate largely regular time dependence of SO_4 production and $CaCO_3$ dissolution. We have reproduced below some of the plots presented by these authors. This is consistent with the bulk of our results.

We should add a word of caution here regarding the predictability of AMD as based on purely physico-chemical models. As can be seen from Fig. 3.1, the biological activity of microorganisms present in the environment adds a whole new dimension to the analysis and could effectively alter the end results in terms of the release time and the amount of acid produced. What we wish to rather emphatically stress, however, is that in spite of the highly nonlinear characteristics of the chemical kinetics involved, the observed processes are very regular. No hallmarks of chaos, quasi-periodicity or intermittency have been found. Thus these phenomena should be very easy to model and predict provided reliable input data are available in terms of initial concentrations, reaction rates, flow rates and the structural properties of the medium. Therein lies the challenge of predictability and we believe that with steady progress in understanding the processes involved in AMD we

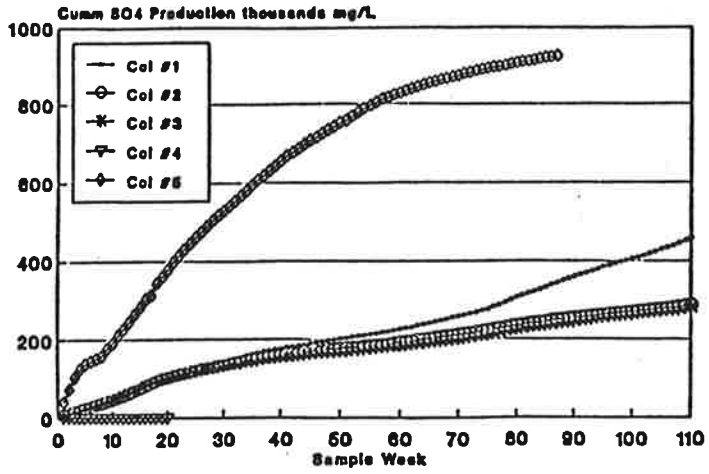

Figure 5.1: Samatosium column leach test following Denholm and Hallan [18].

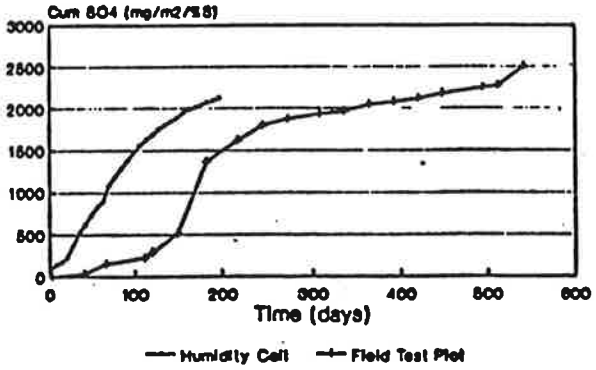

Figure 5.2: Cumulation of SO_4 with time following Ferguson and Morin [20].

should achieve predictability rather sooner than later. Obviously, the model itself is not perfect and several weak points could be identified. We discuss some main areas in need of improvement in Secs. 5.2 and 5.3.

5.2 Future Outlook

In the model developed in the studies presented in this report a major point requiring further improvement is related to the inhomogeneity of the medium. Although we have effectively included porosity through the use of time dependent reaction rates, the other aspect of the problem, i.e. diffusivity of motion of the chemical species still needs to be addressed. It is well known that when there is neither stirring nor sufficient natural convection, molecular diffusion may govern transport and species concentrations may vary from point to point [Gray (1988)]. This would call for the use of time and space dependent

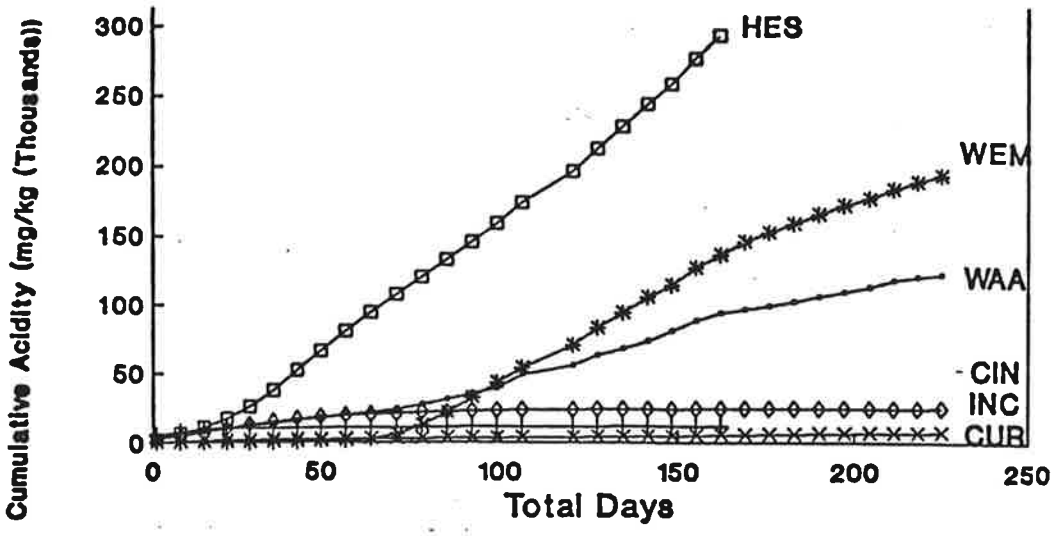

Figure 5.3: Plot of cumulative acidity for acidic weathering cells following Bradham and Caruccio [19].

concentration fields $X_i(t, \underline{x})$ and $Y_j(t, \underline{x})$ in the acid production and acid neutralization reactions studied in this report.

We should mention that Davis and Ritchie [Davis et al. (1986)] have developed a series of models simulating diffusion into rock piles. The initial model, called the simple homogeneous model, simulated oxygen differences from the top of a pile downwards to oxidation sites. The model equations were solved assuming pseudo-steady -state diffusion within the particles. However, this and all the subsequent models[Morin et al. (1990)] were based on a linear diffusion equation of the type:

$$D_3 \left[\frac{d^2C}{dr^2} + \frac{2}{r}\frac{dC}{dr} \right] = R \tag{5.1}$$

Where D_e is the effective diffusion constant, C is the oxygen concentration and R is the rate of O_2 uptake. As demonstrated by Prigogine and many other reseachers [Glansdorff et al. (1971)], a more appropriate description for reaction-diffusion equations calls for the use of nonlinear coupled partial differential equations of the form

$$\frac{\partial \mathbf{u}}{\partial \mathbf{t}} = f(\mathbf{u}) + \mathbf{D}\nabla^2\mathbf{u} \tag{5.2}$$

where D is a diffusion constant [Kuramoto (1984)] and $f(\mathbf{u})$ is a nonlinear function coupling the species involved according to reaction kinetics. Depending on the particulars of the system, a reaction-controlled, a diffusion-controlled or an intermediate regime may prevail. Both oscillatory and chaotic temporal regimes may exist and spatial patterns show amazing complexity exhibiting propagating and standing wave behavior, rotating spiral formation[Henze et al. (1990)] as well as chemical turbulence. Bifurcations are known to occur resulting from unequal diffusion coefficients for the individual reactions. Importantly to our problem, observations of such behavior have been made for heterogeneous processes occurring at gas-solid and liquid-solid interfaces, e.g. catalytic oxidation of CO on Pt (110) single crystal surfaces. In a recent study [Ertl (1991)] it was shown

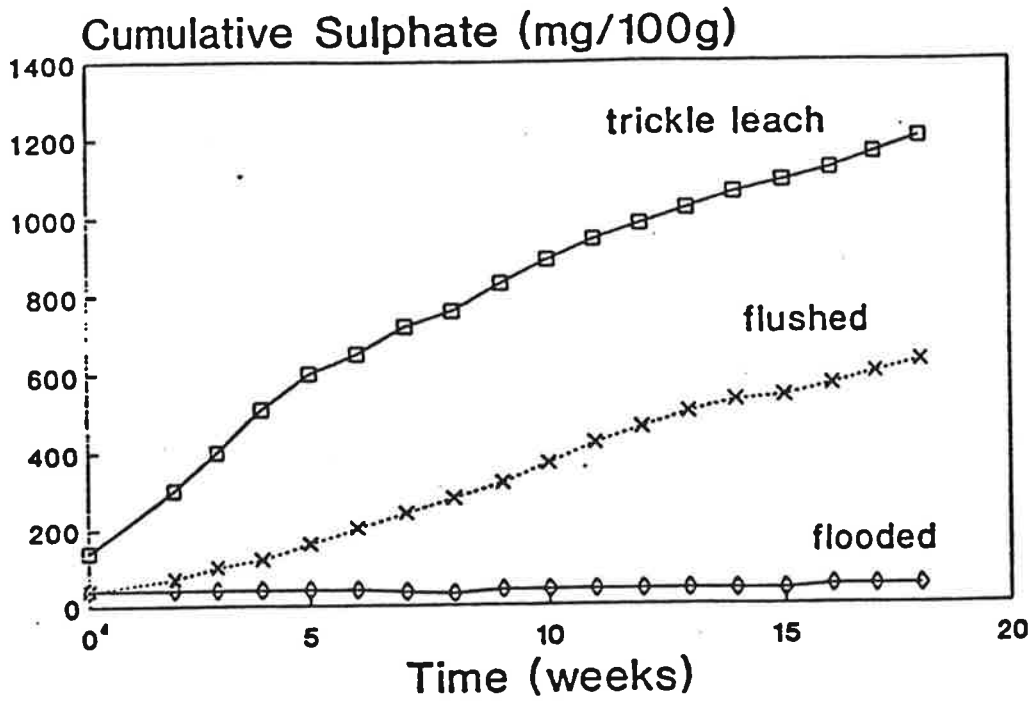

Figure 5.4: Variation of acid generation with leach method following Steffen, Robertson and Kirsten [16].

through computer simulations, scaling arguments and experiments (naphthalene aggregation) that in porous media where interplay between energetic and geometric heterogeneity exists, *fractal* nature of chemical reactions can be seen. We expand on this aspect in Sec. 5.3 below.

Our conclusion, therefore, is to contemplate an extended model of nonlinear chemical kinetics which would account explicitly for diffusion of chemical species, their reactivity as well as the porosity of the medium. Only then can we adequately address quantitative aspects of predictability and prevention in the AMD problem as seen through nonlinear modelling techniques.

In order to provide the reader with some basic information on the complexity of the problem ahead, we have written a subsection dealing with the modelling of rock and flow processes in rock. This should, at the next stage of our model development, be incorporated into the chemical kinetics analyzed here largely as a process in a homogeneous medium which, obviously, is a gross oversimplification.

5.3 Rocks: characterization and flow properties

One of the most important findings of the present paper was the role flow rates and porosity of the rock material may play in the chemical kinetics of the AMD problem. In this concluding section we wish to outline some pertinent points that should be taken into account in future modelling and prediciton of the phenomenon investigated. In what follows we have largely drawn on the excellent recent review of the topic by Sahini (1993).

In the phenomena discussed in this report, a complex pore structure of the medium is in existence and it significantly affects the distribution, flow, mixing and displacement

of fluids present. Various physical mechanisms play a role, such as heat and mass transfer, thermodynamic phase behavior, forces of viscosity, buoyancy, gravity and capillarity making the analysis especially demanding. For reactive fluids, the pore structure of the medium may even change due to the reactions of the fluid with the rock surface. A crucial point to emphasize here is that the analysis performed depends on several length scales over which the porous medium may or may not be regarded as homogeneous.

When there are inhomogeneities in the system that persist over various length scales, the overall behavior is dependent on transport processes (diffusion, conduction, convection) and morphology. The general classes of porous media distinguished are: (a) microscopically disordered but macroscopically homogeneous (characterized by size-independent transport properties) and, (b) macroscopically hetrogeneous (with several types of transport properties).

To model transport processes in porous media, two types of approaches have been adopted: (a) continuum models; and (b) discrete models. However, only in the past fifteen years have modern ideas from statistical physics been applied to flow, dispersion and displacement processes in porous rocks. Such concepts as percolation, fractality, self-similarity and pattern formation are only now being implemented in the procedures used. We will discuss some of the repercussions that follow in the discussion below. For example, the pore volume and pore surfaces of many reservoir rocks are fractal and hence classical laws of physics have to be significantly modified. For instance, Fick's law of diffusion with a constant diffusity is no longer applicable to diffusion processes in fractal systems. Instead, the diffusion coefficient becomes time- and space-dependent.

Porosity of reservoir rocks, ie. the volume fraction of their open space, has either a primary or a secondary origin. Primary porosity is due to the original pore space of the rock while secondary porosity is due to the chemical and physical changes through reactions with water.

The geometry of rock describes the shapes and sizes of its pores or fractures. In a porous medium, the space between its particles are called voids, whereas if the particles themselves are porous, then the void spaces in the particles are called pores. Pores can be divided into two groups: (a) pore bodies where most of the porosity originates, and (b) pore throats which are the channels that connect pore bodies. In a network representation of the pore space, the pore bodies are shown as sites or nodes while throats represent bonds of the network.

The pore size distribution is defined as the probability density-function that gives the distribution of pore volume by an effective pore size. Four main methods of measuring pore-size distributions are: (a) mercury porosimetry; (b) adsorption-desorption experiments; (c) small-angle scattering and (d) nuclear magnetic resonance.

In Fig. 5.5 we have shown a comparison between several types of porous media and theoretical simulation results. Fig. 5.6 illustrates pore-size distibution functions of sample rocks.

Pore-space models are required for calculating transport coefficients, permeability k and other dynamical properties of porous media. The simplest property of a porous medium is its porosity ϕ. Relationships between k and ϕ have been over the years proposed and tested, but there cannot be any general relationship between k and ϕ since there exist porous media with the same ϕ but different k.

In recent years it has been demonstrated that rock and other porous media (see Fig. 5.7) have fractal properties. There are six basic methods of measuring fractal proper-

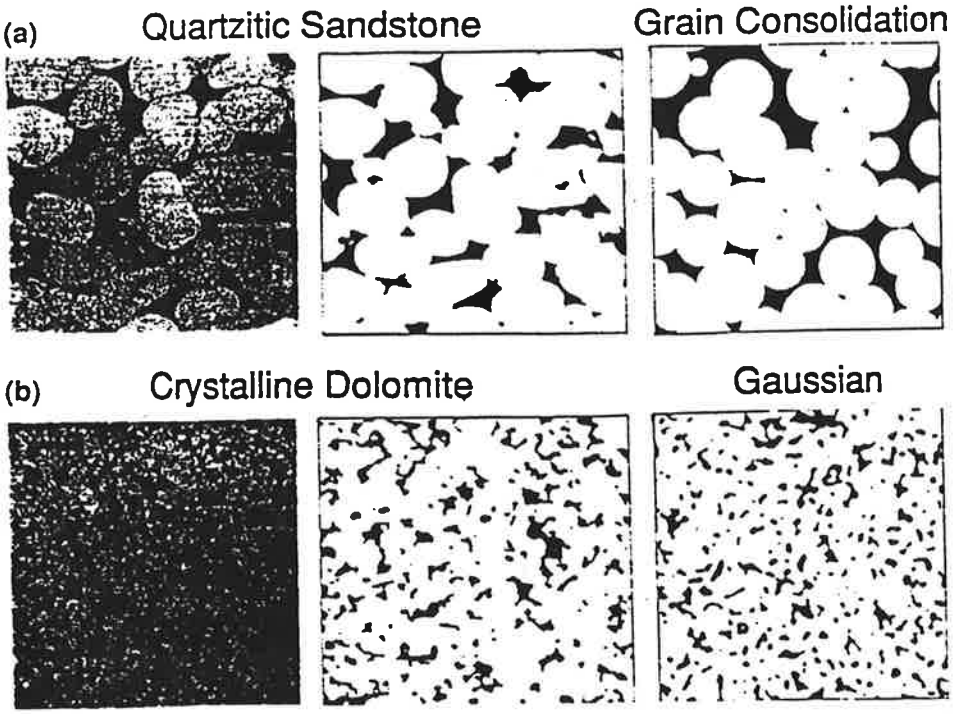

Figure 5.5: Comparison of mathematical models and actual porous media.

ties: (a) the box method; (b) adsorption studies; (c) chord-length measurements; (d) correlation function measurements, (e) small angle scattering and (f) spectral methods.

In addition to fractality of the pores, fractal properties also characterize hetrogeneous and fractured rocks. Fractures provide high permeability patterns for fluid flows and can be parameterized by fracture aperture, ie. the volumetric flow rate through a fracture (as a function of aperture cubed). Fractures in a network appear to have different characteristics than isolated fractures. It was found that the frequency of inverse aperture y as a function of inverse aperture follows a power law, indicating fractality. Fractured rock has fractal geometry and is scale independent so that it can be represented by a singel parameter, the fractal dimension D defined as

$$D = \frac{\log(N_l)}{\log(1/l)} \tag{5.3}$$

where N_l is the number of fractures of length l (see Fig. 5.8).

A study of the literature indicates the existence of three classes of models of fractured rocks: (a) the classical multiporosity model, (b) network models of fractured rocks (fractal models) and (c) multifractal models. Many recent results definitely demonstrate the relevance of fractal statistics to modelling hetrogeneous media and especially transport processes in them. Simulations taking into account fractality lead to substantial improvements in the predictions of process performance. Fractal properties of the medium require the use of scale- and time-dependent dispersion coefficients as, for example, is the case with the typically-used convective diffusion equation

$$\frac{\partial C}{\partial t} + < v > \cdot \nabla C = D_L \frac{\partial^2 C}{\partial x^2} + D_T \nabla_\perp^2 C \tag{5.4}$$

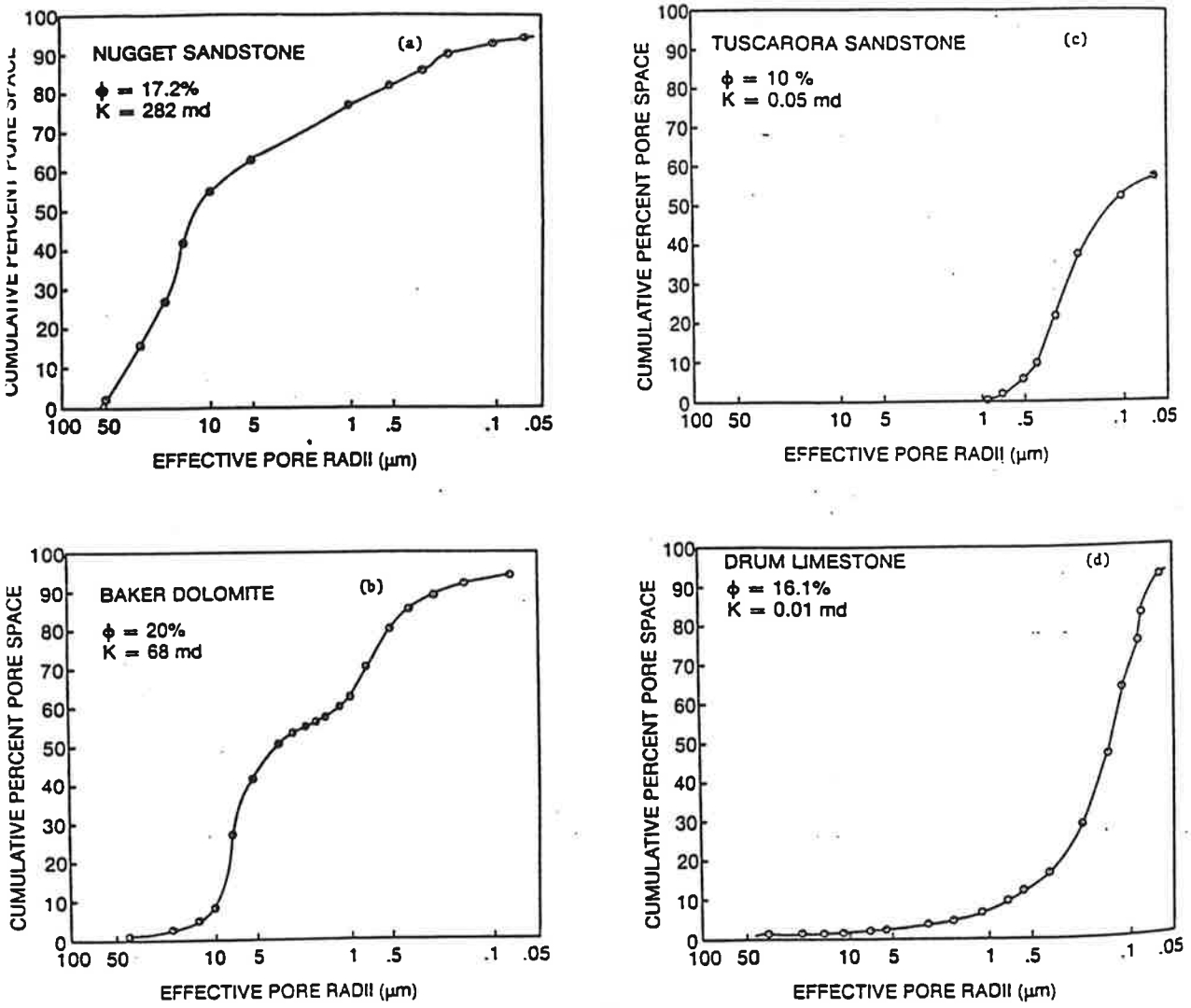

Figure 5.6: Pore-size distribution of various rocks.

where $< v >$ is the macroscopic mean velocity, C the mean concentration of fluid, T and L stand for transverse and longitudinal direction, respectively. It is the objective of modern techniques to determine the dependence of D_L and D_T on the nature of the porous medium present. Monte Carlo simulations demonstrate that dispersion coefficients are scale dependent and for fractal hetrogenities grow with the distance travelled.

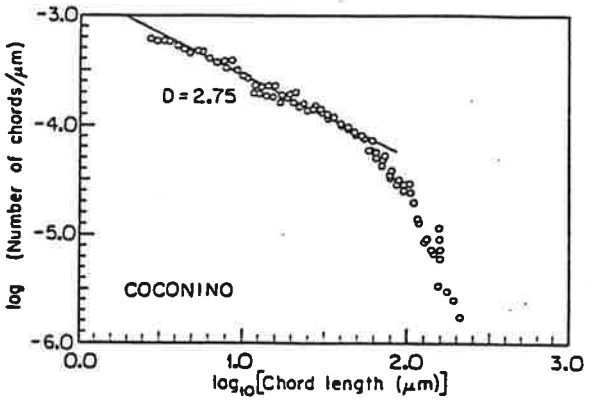

Figure 5.7: Typical fractal plot for Coconino sandstone .

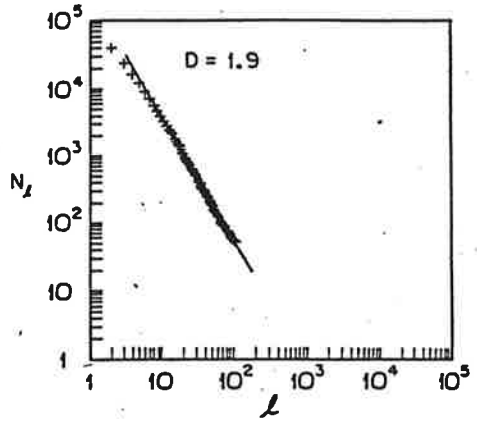

Figure 5.8: Fractal plot of surface fracture pattern.

Acknowledgements

The authors with to thank Mr. B. Godin for his encouragement and for providing them with copies of numerous articles and reports that introduced them to the problem of AMD and its modelling. We also acknowledge valuable input given by Dr. R.V. Nicholson which resulted in significant improvements to the quality of this report.

An Introductory Overview of Nonlinear Phenomena

In the past two decades we have witnessed the emergence of new scientific paradigms that are making a revolutionary impact on the developments in the natural sciences. Such concepts as chaos, strange attractors, limit cycles and fractals are gradually taking root in the vocabulary of leading-edge scientists. The field of chemical kinetics has been an integral part of this new nonlinear science since its beginning. In the sections that follow we provide a non-specialist overview of the key concepts required in the sophisticated modelling of nonlinear chemical kinetics. We begin by introducing the idea of chaotic behavior. This is followed by a subsection on coupled systems and limit cycles. The question of predictability arises naturally and here we give the example of the Lorenz system where predictability is completely impossible. Having introduced these general concepts we proceed to discuss their relevance to chemical kinetics. In order to describe chemical kinetics in porous media we then introduce the concept of a fractal and the associated idea of percolation. The final subsection deals with an emerging paradigm called pattern formation.

A: Chaotic Behavior

In the last few decades, the deterministic viewpoint of modern science has been challenged by the discovery of unstable dynamic, conservative systems with totally unpredictable behavior. The majority of dynamic systems, until a few years ago, were thought to be ruled by deterministic laws and their behavior totally predictable. Unstable systems were considered to be an exception to the rule. However, very simple conservative systems exist with few degrees of freedom which show sensitive dependence on the initial conditions and exhibit regimes of chaotic behavior. Their evolution may become unpredictable in spite of an arbitrarily large amount of information we may have about them. Through it all they are indeed subject to the deterministic laws of classical dynamics! The so-called deterministic chaos arises as a result of simple, well-defined mathematical algorithms or equations, such as the logistic map investigated extensively by M. Feigenbaum [Baker et al. (1990), Cvitanović (1984)]. This is a rather simple iterative equation, i.e.

$$x_{n+1} = r x_n (1 - x_n) \tag{A.1}$$

where r in the range: $0 < r < 4$ is called a control parameter. For values of $r < 3$, the results eventually converge to a steady state called an attractor. However, for values of $r > 3$, the resultant oscillation does not settle down and remains stable, i.e. the behavior is periodic. The two possible values of $x_n(r)$ never converge and the curve $x_n(r)$ shows what

we call a bifurcation. Higher values of the control parameter r produce further splitting and doubling of the periodicities involved. Each period doubling is a bifurcation. If one plots the increasing control parameter r horizontally and the variable x_n vertically, we obtain Fig. A.1. Abruptly, at $r = 3.58$, the result for x_n no longer oscillates periodically but changes in a chaotic fashion. The splittings, which started coming faster and faster for $r > 3$, are now squeezed together and the growth rate seems to take any value at random.

Although for the values of r above r_c chaos and randomness seem to prevail, a further increase of the control parameter, which makes the system even more nonlinear, introduces windows of regularity among chaos which is called intermittency. Computer simulations of the logistic map readily demonstrate (see the inset of Fig. A.1) that the structure is infinitely deep and self-similar. Parts of it, when magnified, show identical patterns, ad infinitum. These patterns (though in this example they come from a one-dimensional system) are a very common characteristic of the dynamic behavior of nonlinear systems leading to chaos and complexity. Bifurcations with successive, infinite period doubling define one of the possible routes to chaos [Baker et al. (1990)].

B: Coupled Systems and Limit Cycles

In chemical applications, in particular, the use of a single quantity (such as the variable x_n) is inadequate as concentrations of several reacting chemical species must be described as independent variables. Here, instead of the well-studied relaxation dynamics characterized by an exponential time evolution towards a steady-state attractor, a completely new type of behavior may arise. Specifically, a pattern of oscillating growth or extinction processes of individual species may be observed to act as a stable attractor. Perhaps the simplest example of such a cyclic population evolution can be found in the Lotka-Volterra model of prey and predator competition. Consider as a simple illustration the populations of wolves (predator) and rabbits (prey) living in an isolated geographic area (e.g. an island) to limit the influences of other factors. Starting with a large population of wolves we readily predict a demise of rabbits as they will soon become an easy prey for the roaming wolves. However, as soon as the rabbit population is decimated, the wolves will face starvation leading to a downturn in their numbers. This, in turn, will allow rabbits to repopulate as they face a diminishing population of starved out wolves. As a consequence, a new phase in the development appears with numerous rabbits but few wolves. That will, of course, lead to a rapid repopulation of wolves and we have thus completed one cycle. This pattern repeats itself periodically.

In mathematical terms, we denote the concentration of each species (for example one type of reacting molecules) using a scalar time-dependent variable, say $x_i(t)$, with $1 \leq i \leq n$ denoting the number of species present. The time evolution of the entire system is then governed by coupled first order differential equations of the general type [Glansdorff et al. (1971), Kuramoto (1984)]

$$\frac{dx_\alpha}{dt} = f_\alpha(\{x_i; 1 \leq i \leq n\}) \tag{B.1}$$

where f_α is in general a function of all the concentrations involved and it usually contains

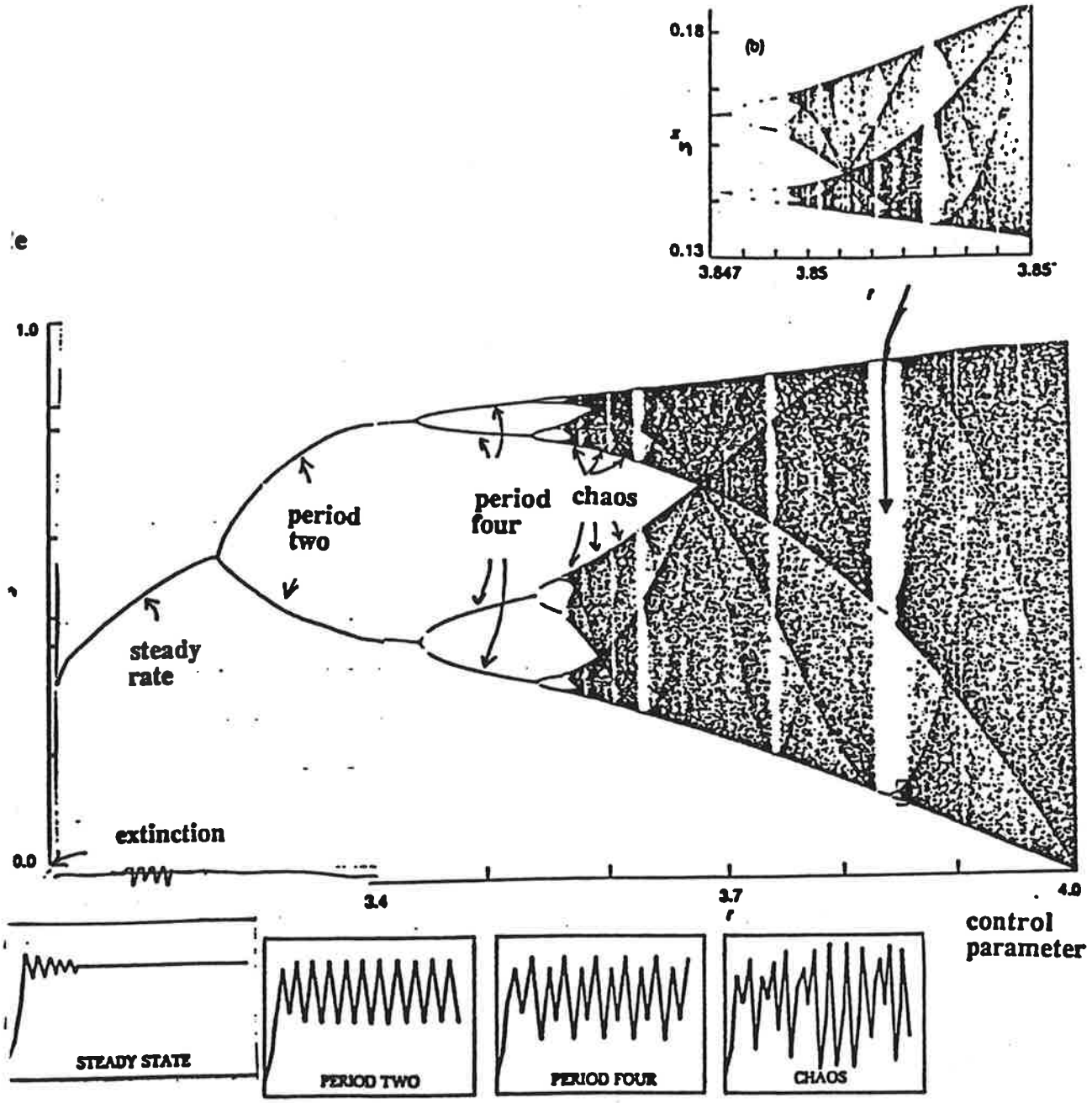

Figure A.1: The logistic map and its properties

significant nonlinearities. Take for example the following simple system [Hale et al. (1991)]

$$\frac{dx_1}{dt} = x_2 + ax_1(x_1^2 + x_2^2) \tag{B.2}$$

and

$$\frac{dx_2}{dt} = x_1 + ax_2(x_1^2 + x_2^2) \tag{B.3}$$

where a is an adjustable constant (a control parameter). In fact, depending on the numerical value of this constant, three completely different types of behavior arise for the solution set: $x_1(t), x_2(t)$. In Fig. B.1 we have shown phase portraits in each case, i.e. plotted the trajectories of $\{x_1(t), x_2(t)\}$ with time t taken as a running parameter. When $a < 0$ a stable focus $x_1 = 0, x_2 = 0$ is found so that all initial conditions lead to a spiralling down on the focus point. When $a = 0$ all the orbits are stable circles since the system can be represented as a harmonic oscillator. Finally, for $a > 0$ an unstable focus appears and all orbits diverge to infinity.

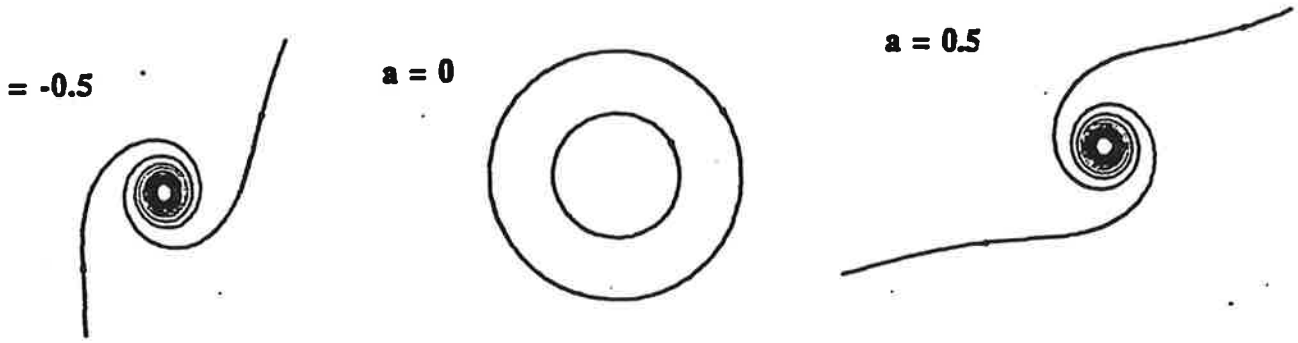

Figure B.1: The three possible behaviors in phase space for the solutions of eqs. (B.2) and (B.3).

I. Prigogine [Prigogine et al. (1968)] studied a trimolecular model for a reaction in an open system that can be schematically described by the reaction chain

$$A \underset{k_{-1}}{\overset{k_1}{\rightleftharpoons}} X \tag{B.4}$$

$$B + X \underset{k_{-2}}{\overset{k_2}{\rightleftharpoons}} Y + D \tag{B.5}$$

$$2X + Y \underset{k_{-3}}{\overset{k_3}{\rightleftharpoons}} 3X \tag{B.6}$$

$$X \underset{k_{-4}}{\overset{k_4}{\rightleftharpoons}} E \tag{B.7}$$

where A, B, D, E, X and Y denote various molecules, k_1, k_2, k_3, k_4 stand for forward while $k_{-1}, k_{-2}, k_{-3}, k_{-4}$ for reverse reaction rates. This system has been referred to as the

Brusselator. In subsection 2.1 of the main text we demonstrate in detail how to derive the associated kinetic equations for the concentrations of X and Y molecules, denoted here for consistency by x_1 and x_2, respectively. They result in

$$\frac{dx_1}{dt} = x_1^2 x_2 - bx_1 + a - x_1 \tag{B.8}$$

and

$$\frac{dx_2}{dt} = -x_1^2 x_2 + bx_1. \tag{B.9}$$

What Prigogine noticed solving these equations (see Fig. B.2) was the presence of a (periodic) closed orbit in the phase space (x_1, x_2) to which all the neighboring trajectories are attracted. He called it a limit cycle and demonstrated its ubiquitous applicability as a self-sustaining pattern of oscillatory behavior. Prigogine's discovery was revolutionary enough to the field of chemical kinetics that he was awarded a Nobel Prize in Chemistry.

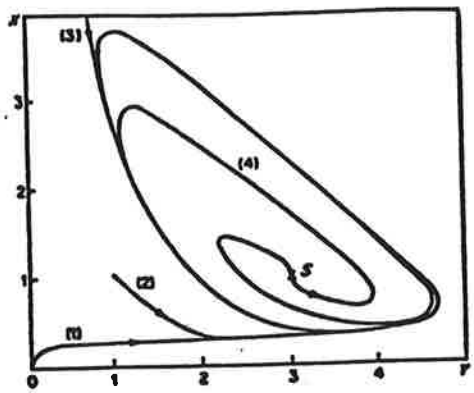

Figure B.2: Trajectories obtained by numerical integration for the Brusselator reactions (B.4)-(B.7) for (1) X=Y=0; (2) X=Y=1; (3) X=10; Y=0; (4) X=1; Y=3.

More complicated nonlinear systems may possess a number of attractors (either point-like or limit cycles) and their trajectories may tend to one or more of them depending on the initial conditions, i.e. their location with respect to the basins of attraction present [Glass et al. (1988)].

It could at first appear that all attractors in nonlinear dynamical systems have rather regular geometries. However, a large class of systems were discovered which display attractors whose geometry is so complicated that it defies description. This is partly why this new type of attractor was called a strange attractor. In the next Appendix we discuss this novel nonlinear phenomenon.

C: Strange Attractors and Prediction Limitations

The MIT meteorologist E. Lorenz worked in the early sixties on simple models of atmospheric convection which results due to the daily operation of the Sun's rays. He managed to simplify the problem to a system of just three coupled differential equations given below

$$\frac{dX}{dt} = \sigma(X - Y) \tag{C.1}$$

$$\frac{dY}{dt} = -rX - Y - XZ \tag{C.2}$$

$$\frac{dZ}{dt} == -bZ + XY \tag{C.3}$$

where σ, r and b are fixed model-dependent parameters and the physical variables X, Y and Z depend on time t. Here, X denotes the intensity of the convection current, Y is the temperature difference at the boundary layers and Z stands for the deviation from a linear vertical temperature profile in the absence of convection. These three equations look deceptively simple even to a non-specialist but they proved to be unsolvable analytically. Lorenz's meticulous numerical work led to his discovery of a very important new concept. He noticed that his computer-generated solutions differed beyond recognition when a seemingly negligible round-off correction was introduced to his input data. This came to be known as the "Butterfly Effect" signifying sensitive dependence of the solutions on the initial conditions. The illustrative hyperbola used was that of a butterfly flapping its wings and thus disturbing the weather pattern at a distant location over a sufficiently long time.

When Lorenz plotted his solutions in the phase space, he obtained sets of trajectories which looked anything but regular. The curve traced by the values of $X(t), Y(t)$ and $Z(t)$ had very peculiar features as can be seen in Fig. C.1.

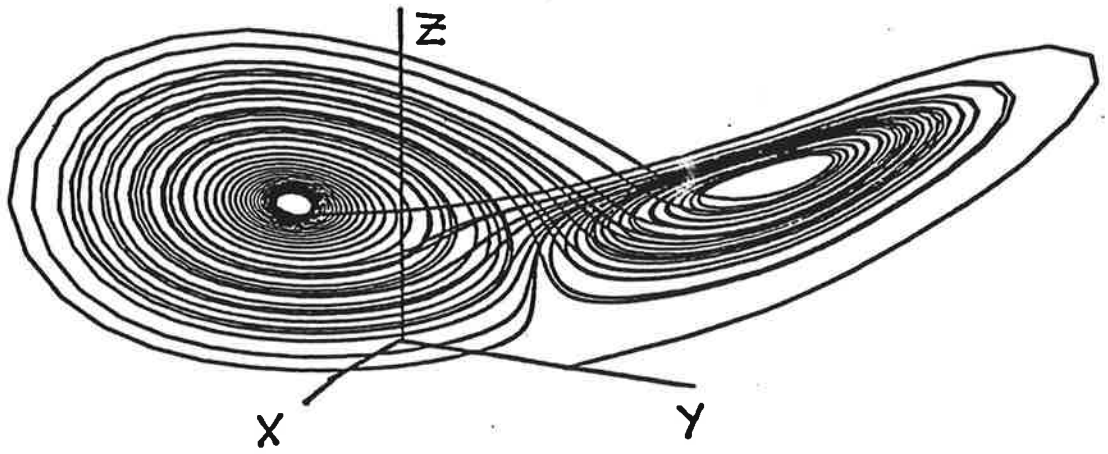

Figure C.1: The strange attractor of Lorenz.

We see in Fig. C.2 a multitude of loops that never repeat themselves and which circle around two areas of phase space switching from one side to the other in an arbitrary fashion. This diagram was called by D. Ruelle a strange attractor. On a closer inspection of the Lorenz attractor we find that its trajectories are infinitely close together but never intersect one another. Any part of the attractor where the spirals seem to join, contains infinite numbers of trajectories. Yet, although the number of trajectories is infinite, the attractor holds the system's dynamics within finite boundaries, the latter being a somewhat contradictory, incompatible term. Indeed, a chaotic attractor is in itself a contradiction: an infinite number of trajectories of infinite length are contained in a finite space. Another important property already mentioned here is its chaotic, random, infinitely complex behavior. This gives rise to unpredictability symbolized by the butterfly

effect concept mentioned earlier. The fractal nature of a strange attractor introduces with it a non-integer dimension. Point attractors are zero-dimensional, limit cycles are of dimension one (curves) and quasi-periodic attractors (tori) are two-dimensional (surfaces). Curiously, the dimensionality of a strange attractor, as in general is the case for a fractal object, is a real, non-integer number, say 1.74. A number like this can be obtained through a rigorous algorithmic limit finding procedure which will be discussed in the next section which deals specifically with fractals. Instead of the traditional time series analysis, phase space trajectories revea l the implicate order present in chaotic dynamics. Fig. C.2 schematically juxtaposes both ways of presenting data for a variety of modes of behavior.

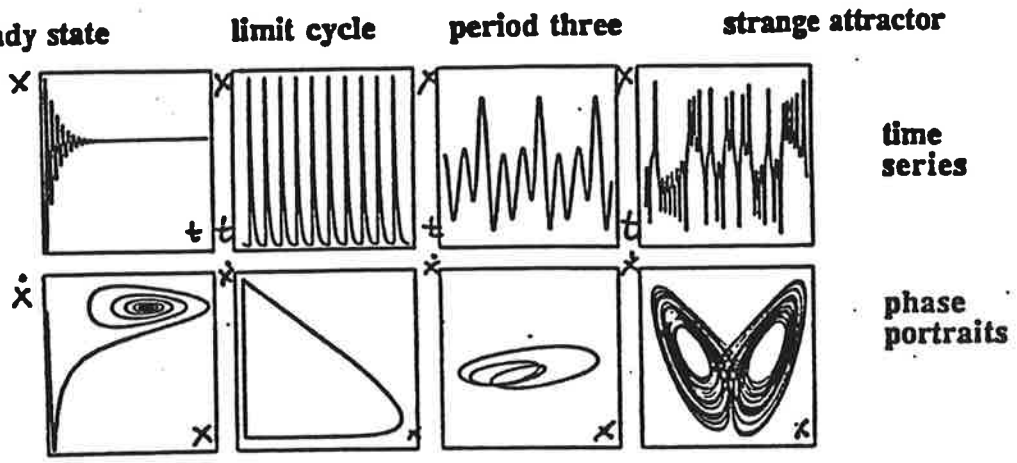

Figure C.2: Time-series versus phase-space characteristics for several nonlinear modes of behavior.

D: Fractals

Many pattern forming systems, especially when they are far from thermodynamic equilibrium, exhibit a growth of forms which are of fractal nature [Feder (1988)]. Specific examples include:

(a) Dendritic solidification in an undercooled medium;

(b) Viscous fingering phenomena which occur when two fluids of different viscosities penetrate each other;

(c) Aggregation phenomena such as diffusion-limited aggregation; and

(d) Electrodeposition patterns of ions onto an electrode.

Some of these examples are graphically illustrated in Fig. D.1.

The basic property of all fractal objects is their self-similarity, i.e. when we cut a part of the object and then magnify it, the resulting objects appear the same as (or at least very similar to) the original object. Another property of fractals, which actually earned them

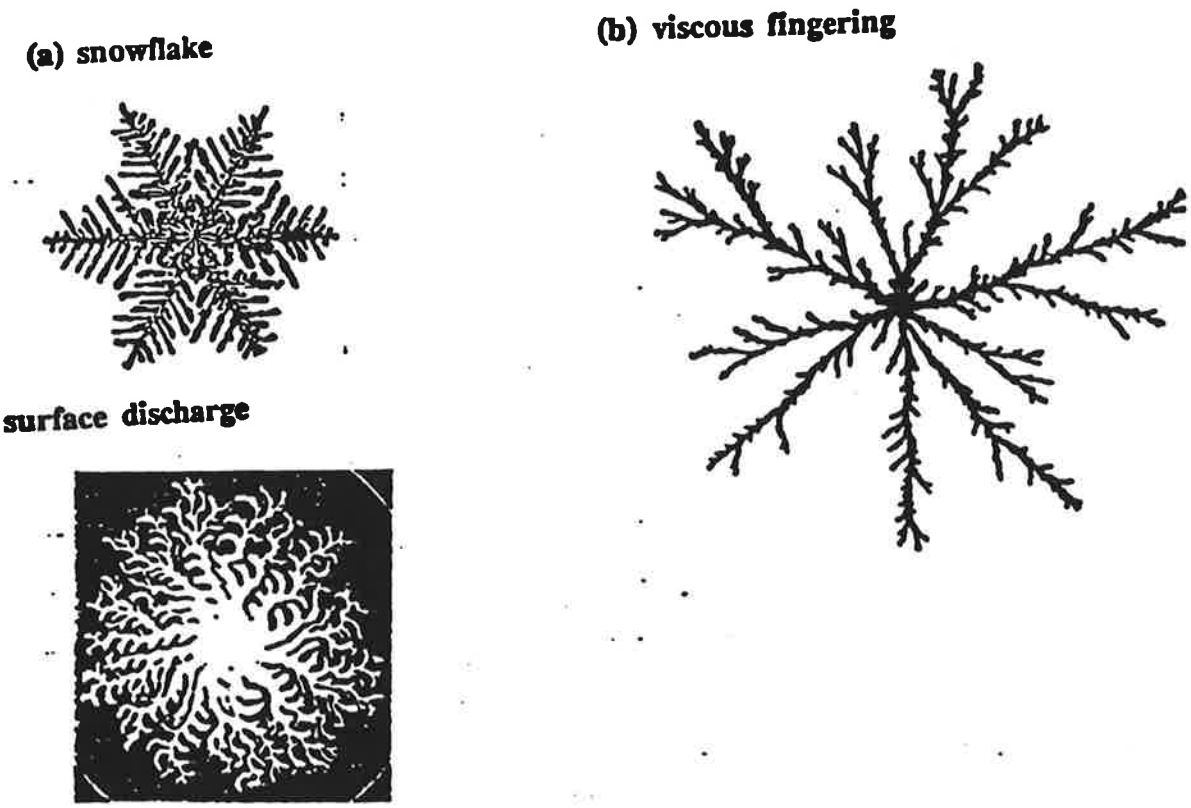

Figure D.1: Examples of fractals in nature.

their name, is that their dimensionality is not an integer but in general a real number. In the simplest form, the so-called fractal dimension D is given by the relationship

$$V(R) \sim R^D \tag{D.1}$$

where $V(R)$ is the volume of the region bounded by the interface whose radius is R. The notion of fractual especially as it pertains to geometrical objects was principally introduced into science by B. Man delbrot. It was subsequently studied by many physicists and generalizations of the definition were proposed, including multi-fractality. In the physical context it is useful to distinguish two general classes of fractals:

(a) deterministic where a simple iterative rule is present, e.g. involving a procedure to cut a part of the object at each stage and replace it with a fixed element, and

(b) random where a stochastic approach is used so that a given operation, e.g. aggregation event, is predicted, with a preselected probability level.

Fractal objects can also be constructed algorithmically in two- or three-dimensional spaces. Two famous examples of fractal objects existing on a plane are the so-called Sierpinski gasket and the Sierpinski carpet (see Fig. D.2).

In a more rigorous sense, a fractal is a set of points in space for which the so-called Hausdorff-Besicovitch dimension D strictly exceeds the topological dimension D_T. While the topological dime nsion is always an integer (1,2 or 3), the fractal dimension D is never an integer but a real number. The latter quantity expresses the property of size scaling

(a) Sierpinski gasket

$$D = \frac{\ln 3}{\ln 2} = 1.58...$$

(b) Sierpinski carpet

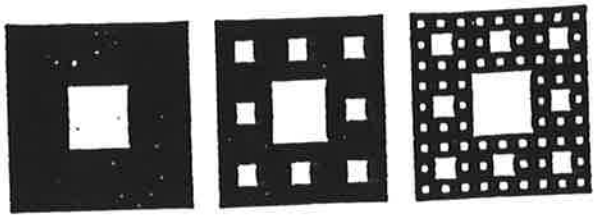

$$D = \frac{\ln 8}{\ln 3} = 1.89...$$

Figure D.2: Two examples of mathematical fractals.

with the distance from the centre of a fractal object. The fractal dimension presents a way of quantifying properties that otherwise would have no clear definition. It expresses the degree of roughness or irregularity of a fractal object. In Figs. D.1 and D.2 we have given the fractal dimensions of the objects illustrated there.

E: Percolation Process

The concept of percolation was originally introduced to deal with the process of spreading of a fluid through a random medium, for example oil or water in the pore space of a rock. In general, the underlying mechanism of randomness in the process can be of 2 different types: (a) the classical diffusion process introduces randomness to the fluid, and (b) the percolation process introduces randomness to the medium's structure.

A site percolation problem is based on a network of lattice sites which are either occupied (probability p) or vacant (probability $1-p$). Two nearest-neighbor sites are called connected if they are both occupied. One similarly defines a connected cluster. There is a site percolation threshold p_{cs} above which an infinite cluster of connected sites spans the network. In addition, one also defines the following important characteristics:

(i) the percolation probability $P(p)$ which characterizes the probability that, when the fraction of occupied bonds is p, a given site belongs to the infinite cluster of occupied bonds.

(ii) the accesible fraction $X^A(p)$ is the fraction of coducting bonds belonging to the infinite cluster.

(iii) the backbone fraction $X^B(p)$ is the fraction of conducting bonds in the infinite cluster which participate in conduction (flow).

(iv) the correlation length $\xi_p(p)$ is the radius of the connected clusters for $p < p_c$ and the length scale over which the percolating network is homogeneous for $p > p_c$.

(v) the average number of clusters of size s, $n_s(p)$

(vi) the effective conductivity of the network, g_e

It has been demonstrated that the above quantities satisfy simple scaling laws

$$P(p) \sim (p - p_c)^{\beta_P} \quad \text{(E.1)}$$
$$X^A(p) \sim (p - p_c)^{\beta_P} \quad \text{(E.2)}$$
$$X^B(p) \sim (p - p_c)^{\beta_P} \quad \text{(E.3)}$$
$$\xi_p(p) \sim (p - p_c)^{-\gamma} \quad \text{(E.4)}$$
$$g_e(p) \sim (p - p_c)^{\mu} \quad \text{(E.5)}$$
$$\text{(E.6)}$$

Since, according to Einstein's relation, the effective diffusivity D_e is related to g_e via $g_e \sim n_e D_e$ (where n_e is the density of particles), we also have

$$D_e(p) \sim (p - p_c)^{\mu - \beta_P}. \quad \text{(E.7)}$$

We conclude that the behavior of percolating networks close to the percolation threshold is insensitive to the lattic structure and to whether the percoloation process is a site or a bond percolation problem.

Fig. E.1 below illustrates some of the scaling relations discussed above.

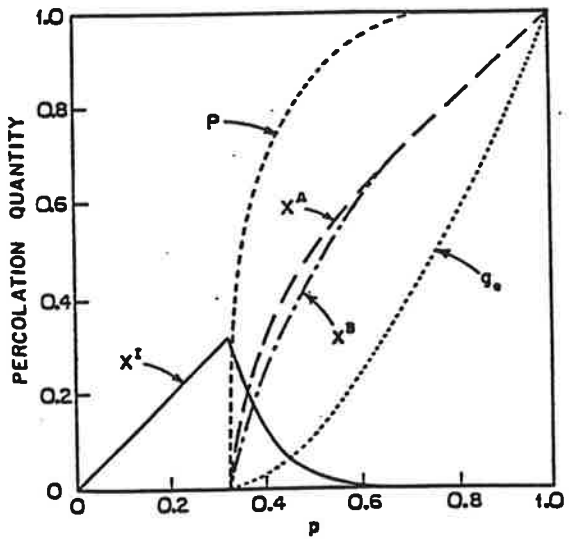

Figure E.1: Typical behavior of some percolation quantities as a function of p, the fraction of occupied sites in a simple cubic lattice.

F: Pattern Formation

A newly emerging paradigm of nonlinear science can be identified as pattern formation and it involves effects in inhomogeneous systems out of thermodynamic equilibrium which are subjected to external forces. Examples of pattern-forming systems are legion and they range from convection in low-dimensional fluids (eg. the Rayleigh-Bénard effect,

the Taylor-Couette flow) to solidification patterns (dendridic growth of the solid helium phase in solution), to chemically-active media (spiral patterns in Belousov-Zhabotinskii reactions), to biological systems (eg. growth patterns in morphogenisis).

Recent progress in the mathematical analysis of nonlinear differential equations, the development of high-speed reliable numerical codes and the associated hardware, as well as the advances made in statistical physics, all made it possible to investigate this broad range of scientific problems within a single unified framework of nonlinearity at work.

The basic assumption is that nonequilibrium spatial patterns may be classified according to the linear instabilities of an infinite, initially spatially uniform system when it is brought away from thermal equilibrium by increasing a given control parameter (eg. the temperature gradient or the flow rate). Generally, the observed instabilities fall into three classes: (a) periodic in space and stationary in time, (b) uniform in space and oscillatory in time. and (c) periodic in space and oscillatory in time.

Traditionally, it has been thought that we should select the state (a solution of the underlying equation of state) that grows fastest with time. However, while commonly true, various other mechanisms are known to exist in pattern selection which restrict the available states. Examples of such effects include: boundaries, parameter inhomogenaities, distortions, noise, etc.. A primary mechanism for pattern selection is through the motion and interaction of defects since they provide a way for a region of space with an "unfavorable" pattern to give way to a more favorable one. It should be stressed that a common feature of pattern-forming systems is the persistence of irregular bahavior (chaos) over long periods of time under fixed external constraints.

Briefly speaking, the methods of analysis applied to these problems include linear stability anaylsis, amplitude equations, perturbation methods, multiple scale expansions, phase equations and a wealth of numerical methods. For more detailed information on these technical aspects the reader is referred to an excellent up-to-date review by Cross and Hohenberg (1993).

We close this brief overview of pattern formation with an example which is pertinent to the subject-matter of this report, ie. a chemically active medium. In the simplest version of the Oregonator model (see Sec. 2), one retains only the concentration X_1 of the autocatalytic species $HBrO_2$ and the concentration X_2 of the transition catalyst in the oxidized state (eg. Fe^{3+}). The chemical dynamics is described using two coupled nonlinear partial differential equations below

$$\frac{\partial X_1}{\partial t} = \gamma f(X_1, X_2) + D_1 \nabla^2 X_1 \tag{F.1}$$

and

$$\frac{\partial X_2}{\partial t} = g(X_1, X_2) + D_2 \nabla^2 X_2 \tag{F.2}$$

where D_1 and D_2 are the corresponding diffusion constants of the species and the functions f, g are defined through

$$f = X_1(1 - X_1) - bX_2 \frac{X_1 - a}{X_1 + a} \tag{F.3}$$

$$g = X_1 - X_2. \tag{F.4}$$

Depending on the values of the model parameters chosen (a, b and γ), a very rich dynamical picture emerges with: oscillatory relaxation bahavior, front and pulse propagation, periodic wave trains, target patterns and even spirals present. In Fig. F.1 we have shown

the formation of spiral patterns as obtained in a computer simulation. Fig. F.2 shows a comparable experimentally-observed pattern.

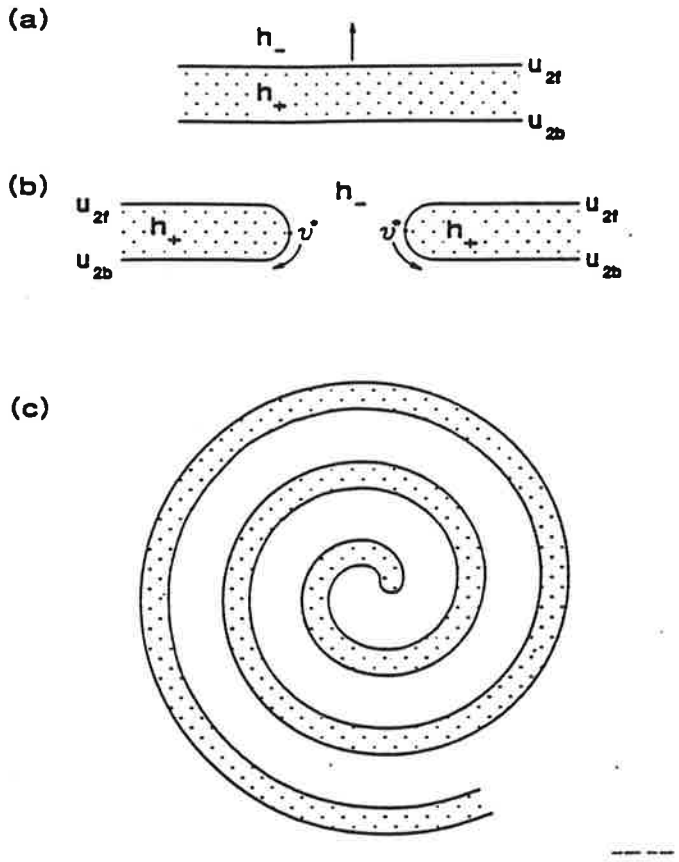

Figure F.1: Schematic illustration of spiral pattern dynamics. (a) and (b) Formation of a spiral by breaking a propagating pulse.

Figure F.2: Spiral patterns in excitable media. (a) Belousov-Zhabotinskii reaction photographed in blue light.

List of Figures

References

[ARDPM] Acid Rock Drainage Prediction Manual (Department of Energy, Mines and Resources, Vancouver, 1990).

[Baker et al. (1990)] G.L. Baker and J.P. Gollub, Chaotic Dynamics (Cambridge Univ. Press, Cambridge, 1990).

[Cvitanović (1984)] P. Cvitanović, Universality in Chaos (Adam Hilger Ltd. Bristol, 1984).

[Glansdorff et al. (1971)] P. Glansdorff and I. Prigogine, Thermodynamic Theory of Structure, Stability and Fluctuations (Wiley-Interscience, London 1971).

[Kuramoto (1984)] Y. Kuramoto, Chemical Oscillations, Waves and Turbulence (Springer, Berlin, 1984).

[Hale et al. (1991)] J. Hale and H. Kocak, Dynamics and Bifurcations (Springer-Verlag, New York, 1991).

[Prigogine et al. (1968)] I. Prigogine and R. Lefevre, J. Chem. Phys. **48**, 1695 (1968).

[Glass et al. (1988)] L. Glass and M.C. Mackey, From Clocks to Chaos (Princeton Univ. Press, Princeton, 1988).

[Feder (1988)] J. Feder, Fractals (Plenum Press, New York, 1988).

[Gray (1988)] P. Gray,"Instabilities and Oscillations in Chemical Reactions in Closed and Open Systems", Proc. Roy. Soc. Lon. A **415**, 1 (1988).

[Richetti et al.] P. Richetti and A. Arneodo, The Periodic-Chaotic Sequences in Chemical Reactions: A Scenario Close to Homoclinic Condition, preprint.

[Vidal et al. (1984)] C. Vidal and A. Pecault (eds.) Non-Equilibrium Dynamics in Chemical Systems (Springer, Berlin, 1984).

[Kopelman (1986)] R. Kopelman, J. Stat. Phys. **42**, 185 (1986).

[DARDTG v.1] Draft Acid Rock Drainage Technical Guide Vol. 1 (British Columbia Acid Mine Drainage Task Force, Vancouver, 1989).

[RPWQM Rep. No. 195201] Rock Pile Water Quality Modelling. Report No. 195201, Steffen, Robertson and Kirsten, Oct. 1992.

[Otwinowski (1993)] M. Otwinowski, Quantitative Analysis of Chemical and Biological Kinetics for the Acid Mine Drainage Problem, preliminary progress report (1993).

[Denholm (1991)] E. Denholm and R. Hallan, a review of Acid Generation Research at the Samatosum Mine, in 1991 MEND Conference Proceedings, Montreal, Sept. 16-18, 1991, Vol. **2**, p.561.

[Bradham et al.] W.S. Bradham and F.T. Caruccio. a Comparative Study of Tailings Analysis Using Acid Base Accounting, Cells, Columns and Soxhlets, ibidem, Vol.**1**, p.157.

[Ferguson et al.] K.D. Ferguson and K.A. Morin, The Prediction of Acid Rock Drainage - Lessons from the Data base, ibidem, Vol. **3**, p.83.

[Henze et al. (1990)] C. Henze, E. Lugosi and A.T. Winfree, Can. J. Phys. **68**, 683 (1990).

[Ertl (1991)] G. Ertl, Science **254**, 1750 (1991).

[Davis et al. (1986)] G.B. Davis and A.I.M. Ritchie, Appl. Math. Model. **10**, 314; 323 (1986).

[Morin et al. (1990)] K.A. Morin, E. Gevencher, C.E. Jones, D.E. Konasewich, J.R. Harries, Critical Literature Review of Acide Drainage From Waste-Rock. Draft Report, May 1990.

[Cross et al. (1993)] M.C. Cross and P.C. Hohenberg, Rev. Mod. Phys. **65**, 851 (1993).

[Sahini (1993)] M. Sahini, Rev. Mod. Phys. **65**, 1393 (1993).

[Jaynes et al. (1984)] D.B. Jaynes, A.S. Rogourski and H.B. Pionke, Water Resources Research **20**, 233 (1984).

[Scharer et al. (1993)] J.M. Scharer, R.V. Nicholson, B. Halbert and W.J. Snodgrass, A Computer Program to Assess Acid Generation in Pyritic Tailings, Proc. ACS Symposium of Environmental Geochemistry of Sulphide Oxidation (1993).

[Doepker et al.(1991)] R.D. Doepker and P.L. Drake, Laboratory Study of Submerged Metal-Mine Tailings 3: Factors Influencing the Dissolution of Metals, Proc. Second Int. Conf. on the Abatement of Acid Drainage, Vol 1 (1991)